Available online at www.sciencedirect.com

ScienceDirect

Nuclear Physics B 923 (2017) 350–377

NUCLEAR PHYSICS B

www.elsevier.com/locate/nuclphysb

Quantum stabilization of a hedgehog type of cosmic string

M. Quandt [a], N. Graham [b], H. Weigel [c,*]

[a] *Institute for Theoretical Physics, University of Tübingen, D-72076 Tübingen, Germany*
[b] *Department of Physics, Middlebury College, Middlebury, VT 05753, USA*
[c] *Institute for Theoretical Physics, Stellenbosch University, Matieland 7602, South Africa*

Received 25 June 2017; received in revised form 25 July 2017; accepted 31 July 2017
Available online 7 August 2017
Editor: Stephan Stieberger

Abstract

Within a slightly simplified version of the electroweak standard model we investigate the stabilization of cosmic strings by fermion quantum fluctuations. Previous studies of quantum energies considered variants of the Nielsen–Olesen profile embedded in the electroweak gauge group and showed that configurations are favored for which the Higgs vacuum expectation value drops near the string core and the gauge field is suppressed. This work found that the strongest binding was obtained from strings that differ significantly from Nielsen–Olesen configurations, deforming essentially only the Higgs field in order to generate a strong attraction without inducing large gradients. Extending this analysis, we consider the leading quantum correction to the energy per unit length of a hedgehog type string, which, in contrast to the Nielsen–Olesen configuration, contains a pseudoscalar field. To employ the spectral method we develop the scattering and bound state problems for fermions in the background of a hedgehog string. Explicit occupation of bound state levels leads to strings that carry the quantum numbers of the bound fermions. We discuss the parameter space for which stable, hedgehog type cosmic strings emerge and reflect on phenomenological consequences of these findings.

* Corresponding author.
E-mail addresses: markus.quandt@uni-tuebingen.de (M. Quandt), ngraham@middlebury.edu (N. Graham), weigel@sun.ac.za (H. Weigel).

http://dx.doi.org/10.1016/j.nuclphysb.2017.07.022

1. Introduction and motivation

The electroweak standard model and many of its extensions have the potential to support string-like configurations. These field configurations are the particle physics analogs of vortices or magnetic flux tubes in condensed matter physics. They are usually called *cosmic strings* to distinguish them from the fundamental variables in string theory, and also to indicate that they typically stretch over cosmic length scales. In the context of the standard model they are also called Z (or W) strings [1–3] to illustrate that are composed of massive gauge fields.

The topology of string-like configurations is described by the first homotopy group $\Pi_1(\mathscr{M})$, where $\mathscr{M}$ is the manifold of vacuum field configurations far away from the string. In typical electroweak-type models, a Higgs condensate breaks an initial gauge group G down to some subgroup H, so that $\mathscr{M} \simeq G/H$. Topologically stable strings are therefore ruled out in the electroweak standard model $SU(2) \times U(1) \to U(1)$ because G/H is simply connected. Nevertheless, one could envision a GUT and/or supersymmetric extension in which a simply connected group G breaks down to the electroweak $SU(2) \times U(1)$ at a much higher scale, so that $\Pi_1(G/(SU(2) \times U(1)))$ is nontrivial and strings would be topologically stable in such GUTs. These strings would have enormous energy densities, so that they could be seen by direct observation using gravitational lensing [4,5] or by signatures in the cosmic microwave background [6].

The absence of topological stability does not imply that the Z strings at the electroweak scale are unstable or irrelevant for particle physics. While their direct gravitational effects are small, Z-strings can still be relevant for cosmology at a sub-dominant level [7,8]. Their most interesting consequences originate, however, from their coupling to the standard model fields. Z-strings provide a source for primordial magnetic fields [3] and they also offer a scenario for baryogenesis with a second order phase transition [9]. In contrast, a strong first order transition as required by the usual bubble nucleation scenario is unlikely in the electroweak standard model [10] without non-standard additions such as supersymmetry or higher-dimensional operators [11]. When a string changes its shape baryon number violation may occur, but for baryogenesis to prevail after the string has disappeared an additional process, *e.g.* via a sphaleron transition, is required [12]. Also de-linking closed Z-strings changes their helicity (Chern–Simions number) which in turn induces baryon number violation [13]. Yet, the baryon number generation from Z strings is not sufficient to explain the observed abundance [14].

However, such effects are only viable if the cosmic strings are at least meta-stable, such that they live long enough to have a cosmological impact. Classically, the energy required to wind up an electroweak string of astrophysical length scales is huge, but it may eventually be overcome by quantum effects induced by the coupling to the remaining fields. In this respect, the most important contributions are expected to come from heavy fermions, since their quantum energy dominates in the limit $N_C \to \infty$, where N_C is the number of QCD colors or other internal degrees of freedom. Heavier fermions are expected to provide more binding since the energy gain per fermion charge is higher and their Yukawa coupling to the string is larger; a similar conclusion can also be drawn from decoupling arguments [15]. Generally, the string background deforms the Dirac spectrum and typically leads to the formation of either an exact or near zero mode [16], so that fermions can substantially lower their energy by binding to the string, which may eventually overcome the classical energy cost of building the string. For consistency, however, one must include *all* contributions which have the same formal loop order; in particular, this means that the deformation of the continuous part of the spectrum (the vacuum polarization energy) must be taken into account as well.

A number of previous studies have investigated quantum properties of string configurations. Naculich [17] has shown that in the limit of weak coupling, fermion fluctuations destabilize the string. The quantum properties of Z-strings have also been connected to non-perturbative anomalies [18]. The emergence or absence of exact neutrino zero modes in a Z-string background and the possible consequences for the string topology were investigated in Ref. [19]. A first attempt at a full calculation of the fermionic quantum corrections to the Z-string energy was carried out in ref. [20]. In that work, the authors could not compare the cosmic string to the perturbative vacuum because of the non-trivial winding of the string background at spatial infinity. Methods to overcome that technical problem were developed a decade later [21,22]. The first comprehensive calculation of the fermionic vacuum polarization energy of the Abelian Nielsen–Olesen vortex [23] has been estimated in ref. [24], where subtractions were carried out in the heat-kernel expansion, which is not easily connected with the standard perturbation counterterms. Quantum energies of bosonic fluctuations in string backgrounds were calculated in ref. [25]. Finally, the dynamical fields coupled to the string can also result in (Abelian or non-Abelian) currents running along the core of the string. The time evolution of such structured strings was studied in ref. [26], where the current was induced by the coupling to an extra scalar field. Circular strings of this type (*vortons*) will acquire an angular momentum that may lead to stabilization [27]; a similar effect can be achieved without extra fields through quantum fluctuations [28]. Other notable scenarios include thermal baths of photons [29], or couplings to invisible (scalar) sectors [30].

Mathematically, the problem of computing the leading quantum energy of a string background amounts to the computation of the determinant for the Dirac operator within this background. Previously, we have employed the *spectral method* to study the quantum energy of a special type of cosmic string in a reduced version of the standard model [31,32]. Even though we allowed for a non-trivial gauge-field structure in the cosmic string background, the findings from Ref. [32] indicate that the preferred string configuration has very little gauge field admixture. Instead, it reduces to a narrow ditch carved in the Higgs condensate. In the present study, we will follow up on the observation that the Higgs field is the dominating factor but consider a different mechanism, inspired by topological solitons, in order to produce attraction in the scalar potential for the fermions and thus generate binding for the fermions. In many non-linear bosonic models such as the Skyrme model [33], the classical solutions of the field equations (*i.e.* the static configurations with minimal energy) that support an extended region of suppressed condensate have a characteristic *hedgehog* structure. When coupled to fermions, as *e.g.* in the Nambu–Jona–Lasinio soliton model [34], the hedgehog configuration produces strong binding even when the magnitude of the scalar component of the Higgs field is homogeneous. Hence this configuration may contribute a significantly lower classical energy for the same gain from the fermion quantum energy. We formulate the two dimensional analog of the hedgehog configuration in the plane perpendicular to the string and extend it uniformly along the string. We couple fermions to this configuration and compute the resulting spectrum. After proper renormalization this spectrum yields the vacuum polarization energy, the numerical simulation of which will determine whether or not such hedgehog structures with shallow scalar Higgs components are energetically favored.

This paper is organized as follows: In the next section we describe our model and introduce the hedgehog type of string configuration. In section 3, we adapt methods from Refs. [31,32] to compute the fermion vacuum polarization energy to this hedgehog configuration. This calculation requires finding the Jost determinant from scattering data and, via the Born series, combining the spectral method with explicit calculations of low-order Feynman diagrams. Then the quantum energy can be renormalized with conventional ($\overline{MS}$ or *on-shell*) schemes, allowing for the

model parameters to be specified from phenomenological data. In that section we also explain how the string is equipped with charge.

In section 4, we present our results for both neutral and charged strings. We also relax our string background profile to allow for a more shallow suppression of the scalar component of the Higgs background, which has smaller classical costs but also tends to bind the majority of fermions less deeply. In our variational approach the optimal configuration for each given charge is selected from several hundred distinct string profiles, and the minimal fermion mass required for a stable configuration is estimated. In section 5, we briefly summarize and discuss our findings and comment on possible consequences for cosmology or particle physics. The technicalities of the scattering problem and the renormalization procedure are described in detail in appendices.

2. Cosmic strings in a simplified electroweak model

A cosmic string is a line-like soliton within electroweak or grand unified type theories. If the gauge group is simply connected ($\pi_1(G) = \emptyset$), there is no topological argument in favor of (classical) stability, and the string must be stabilized dynamically, *e.g.* by reducing its energy via quantum fluctuations. In Ref. [32], we have studied this scenario in a slightly simplified version of the $SU(2)$ electroweak theory,

$$\mathcal{L} = -\frac{1}{2}\,\mathrm{tr}\left(G^{\mu\nu}\,G_{\mu\nu}\right) + \frac{1}{2}\,\mathrm{tr}\left(D_\mu\Phi\right)^\dagger\left(D^\mu\Phi\right) - \frac{\lambda}{2}\,\mathrm{tr}\left(\Phi^\dagger\Phi - v^2\right)^2 + \\ + i\,\bar{\Psi}\left(\mathsf{P}_L\,\not{D} + \mathsf{P}_R\,\not{\partial}\right)\Psi - f\,\bar{\Psi}\left(\Phi\,\mathsf{P}_R + \Phi^\dagger\,\mathsf{P}_L\right)\Psi\,. \tag{1}$$

Here, the first three terms describe the bosonic sector made up of weak gauge bosons W_μ with non-Abelian field strength $G_{\mu\nu} = \partial_\mu W_\nu - \partial_\nu W_\mu + ig[W_\mu, W_\nu]$, and gauge coupling g as well as the Higgs doublet Φ in the fundamental representation of the weak isospin group $SU(2)$. The fourth and fifth terms denote the fermion sector with the minimal coupling of the left-handed quarks to the bosonic sector. Both, the Higgs and the fermion fields couple to the gauge bosons via the covariant derivative $D_\mu = \partial_\mu - igW_\mu$. The simplifications of Eq. (1) as compared to the standard model are: **(i)** the Weinberg angle is set to zero and the $U(1)$ hypercharge is discarded, **(ii)** the fermion doublet is taken to be degenerate in mass with inter-family fermion mixing neglected, **(iii)** only the heaviest quark doublet is retained, since it has the strongest coupling to the Higgs field; see Ref. [32] for further details on the justification of these assumptions.

The string configuration is translationally invariant and is infinitely extended along its symmetry axis. We adapt an *ansatz* that has the typical string-like suppression of the Higgs condensate in the vicinity of the symmetry axis, with no gauge field, *i.e.* $W_\mu = 0$, since previous studies have shown that gauge fields contribute very little to the string binding [32]. The suppression of the Higgs condensate defines the string core. In contrast to the Nielsen–Olesen configuration, the component of the Higgs field which carries the azimuthal dependence, *i.e.* the winding, decays asymptotically for the background that we entertain here. This difference from the Nielsen–Olesen string is due to the non-Abelian character of our model and allows us to indeed set $W_\mu = 0$, because there is no need to compensate for the gradients of the Higgs field at spatial infinity.[1] However, we now require independent profile functions for the charged and neutral Higgs fields in the plane perpendicular to the symmetry axis, which we take to be the z-axis with polar

[1] A Higgs winding at spatial infinity could be introduced by means of a suitable gauge transformation, which would also induce a non-vanishing gauge field in the background.

coordinates r and φ in the xy-plane. Then the two profile functions $\rho(r)$ and $\theta(r)$, called chiral radius and chiral angle, respectively, parameterize the Higgs field in its matrix representation via

$$\Phi = v\,\rho(r) \begin{pmatrix} \cos\theta(r) & i e^{i\varphi} \sin\theta(r) \\ i e^{-i\varphi} \sin\theta(r) & \cos\theta(r) \end{pmatrix}, \tag{2}$$

which is related to the common doublet notation by

$$\varphi = \begin{pmatrix} \varphi_+ \\ \varphi_0 \end{pmatrix} \qquad \Longleftrightarrow \qquad \Phi = \begin{pmatrix} \varphi_0^* & \varphi_+ \\ -\varphi_+^* & \varphi_0 \end{pmatrix}. \tag{3}$$

The string background can then be re-written in the form

$$\Phi = v \left[s(r) + i\,(\boldsymbol{\tau}\cdot\hat{\boldsymbol{r}})^*\, p(r) \right] \tag{4}$$

where $\boldsymbol{\tau}$ are the isospin Pauli matrices. This defines the scalar and pseudo-scalar profile functions

$$s(r) = \rho(r)\,\cos\theta(r) \qquad \text{and} \qquad p(r) = \rho(r)\,\sin\theta(r)\,, \tag{5}$$

which illuminate the relation to the Skyrme model,[2] justifying the identification of our configuration as a hedgehog background.

The vacuum expectation value (*vev*) of the Higgs doublet is at the minimum of the potential, *i.e.*

$$\langle \|\varphi\|^2 \rangle = \langle |\varphi_0|^2 + |\varphi_+|^2 \rangle = \langle \det(\Phi) \rangle = \frac{1}{2} \mathrm{tr} \langle \Phi^\dagger \Phi \rangle = v^2\,. \tag{6}$$

(Note that our convention differs slightly from the standard one, which parameterizes the classical minimum as $\frac{\mu^2}{2}$.) The Yukawa coupling to the quarks gives rise to the quark mass $m = vf = \mu f/\sqrt{2}$. Phenomenologically, the standard Higgs scale is $\mu = 246\,\mathrm{GeV}$, so that $v = 174\,\mathrm{GeV}$. For the top quark this corresponds to a Yukawa coupling of

$$f(\mathrm{top}) = \frac{173\ \mathrm{GeV}}{174\ \mathrm{GeV}} = 0.99\,. \tag{7}$$

The Higgs coupling λ determines the ratio of the Higgs mass and *vev*. More precisely, our convention for the potential gives $m_H^2 = 4\lambda v^2$ and hence

$$\lambda = \frac{m_H^2}{4\,v^2} = \frac{(125\ \mathrm{GeV})^2}{4(174\ \mathrm{GeV})^2} = 0.129\,. \tag{8}$$

It should be stressed again that the two couplings, f and λ, are dimensionless and independent: once the Higgs *vev* is fixed, the Yukawa coupling determines the fermion mass, and the Higgs coupling determines the Higgs mass. In particular, λ is completely obtained from properties of the Higgs field alone. It is therefore convenient to leave the Higgs sector fixed with $\lambda = 0.129$, and vary the Yukawa coupling from its top quark value, Eq. (7) to study the effect of different quark masses.

The classical energy per unit length of the string configuration (4) is obtained by substituting the profiles, Eq. (2), into the (negative) Lagrangian, Eq. (1), integrating over space, and dividing by the (infinite) length, L_z of the string:

[2] It should be emphasized, however, that the Skyrme equations are merely a motivation and the configuration (2) is *not* necessarily a solution of the equations of motion for the model eq. (1), nor is this necessary for the following.

$$\begin{aligned}\frac{\mathcal{E}_{\rm cl}}{m^2} &= \frac{E_{\rm cl}/L_z}{m^2} \\ &= \frac{2\pi}{f^2}\int_0^\infty dr\, r\left(\frac{\rho(r)^2}{r^2}\sin^2\theta(r) + \rho(r)^2\theta'(r)^2 + \rho'(r)^2 + \frac{\lambda}{f^2}\left[1-\rho(r)^2\right]^2\right) \\ &= \frac{2\pi}{f^2}\int_0^\infty dr\, r\left(\frac{p(r)^2}{r^2} + s'(r)^2 + p'(r)^2 + \frac{\lambda}{f^2}\left[1-s(r)^2-p(r)^2\right]^2\right). \end{aligned} \tag{9}$$

Here and in the following, all dimensionful quantities are measured in appropriate units of the quark mass m: for instance, the dimensionless radial distance r in eq. (9) is really $\hat{r} \equiv mr$, but we omit the hat for simplicity.

We require that the background configuration has finite classical energy (per unit length). At large distances from the string core, this implies that the Higgs is in its vacuum state ($\rho = 1$), and $\sin\theta = 0$ to avoid the logarithmic divergence in the first term under the integral in Eq. (9). Unless $\sin\theta \to 0$ as $r \to 0$, the same term has divergences at short distances because we want to allow $\rho(0) = \rho_0$ to take any value. Altogether, the requirement of finite energy enforces the following boundary conditions for the two profile functions in our configuration:

$$\begin{aligned} r\to 0: \quad & \rho(r)\to\rho_0 \qquad \theta(r)\to \nu_0\pi \qquad (\nu_0\in\mathbb{Z}) \\ & s(r)\to\mp\rho_0 \qquad p(r)\to 0 \\ r\to\infty: \quad & \rho(r)\to 1 \qquad \theta(r)\to\nu_\infty\pi \qquad (\nu_\infty\in\mathbb{Z}) \\ & s(r)\to\pm 1 \qquad p(r)\to 0\,. \end{aligned} \tag{10}$$

The integer numbers in the boundary condition for the chiral angle are conventionally chosen as $\nu_0 = -1$ and $\nu_\infty = 0$, leading to the upper sign in the boundary values for the scalar profile $s(r)$. For most of this study, we will assume that the Higgs condensate vanishes at the string core, $\rho_0 = 0$, since this leads to deeply bound fermion states located near the string core, which is beneficial for a possible quantum stabilization. Alternatively, more shallow configurations with $0 < \rho_0 < 1$ induce less binding in the quantum energy, but also have a smaller classical energy to overcome, so that an attractive net effect may emerge as motivated in the introduction.

3. Quantum corrections to the string energy

In the limit of a large number of external quantum numbers (*e.g.* the number of quark colors $N_c \gg 1$), the leading quantum corrections to the classical energy of the cosmic string originate from the fluctuations of the Dirac fermion Ψ. For time-independent background fields, this sector is governed by the single-particle Hamiltonian

$$H = -i\boldsymbol{\alpha}\cdot\boldsymbol{\nabla}\otimes\mathbf{1}_I + \frac{f}{2}\beta\left(\Phi+\Phi^\dagger\right) + \frac{f}{2}\beta\gamma_5\left(\Phi-\Phi^\dagger\right), \tag{11}$$

where $\boldsymbol{\alpha}$, β and γ_5 are the usual Dirac matrices and $\mathbf{1}_I$ is the (2×2) unit matrix in weak isospin space. The entire Hamiltonian acts on 8-component Dirac $\times$ isospin spinors. We split the Dirac Hamiltonian in a free and interaction part, $H = H_0 + H_{\rm int}$, with

$$H_0 = \Big[-i\boldsymbol{\alpha}\cdot\hat{\boldsymbol{r}}\,\partial_r - i\left[\boldsymbol{\alpha}\cdot\hat{\boldsymbol{\varphi}}\,\frac{1}{r}\,\partial_\varphi - i\,\boldsymbol{\alpha}\cdot\hat{\boldsymbol{z}}\,\partial_z + \beta m\right]\Big]\otimes\mathbf{1}_I \tag{12}$$

$$H_{\text{int}} = \beta\left(\frac{f}{2}\left[\Phi + \Phi^\dagger\right] - \mathbf{1}_I\right) + \beta\,\gamma_5\frac{f}{2}\left[\Phi - \Phi^\dagger\right]$$
$$= \beta \otimes \mathbf{1}_I\left[s(r) - 1\right]m + i\,(\beta\gamma_5) \otimes I_\varphi\, p(r)\, m\,, \tag{13}$$

where the Dirac and isospin matrices in the interaction are given explicitly by

$$\beta = \begin{pmatrix} \mathbf{1} & 0 \\ 0 & -\mathbf{1} \end{pmatrix}, \qquad \beta\,\gamma_5 = \begin{pmatrix} 0 & \mathbf{1} \\ -\mathbf{1} & 0 \end{pmatrix}, \qquad I_\varphi \equiv \left(\boldsymbol{\tau}\cdot\hat{\boldsymbol{r}}\right)^* = \begin{pmatrix} 0 & e^{i\varphi} \\ e^{-i\varphi} & 0 \end{pmatrix}. \tag{14}$$

Form the boundary conditions, Eq. (10) we observe that $H_{\text{int}} \to 0$ as $r \to \infty$. This differs significantly from configurations that are variants of the Nielsen–Olesen string and approach a pure gauge configuration asymptotically. This difference simplifies the computation considerably, since no auxiliary gauge field is needed to map this pure gauge onto the trivial configuration [21].

We have omitted the trivial part $(-i\alpha_3\partial_z) \otimes \mathbf{1}_I$ in H_0, since the background is translationally invariant in z-direction. It produces the factor $\sim e^{ipz}$ for the full wave functions and its contribution to the vacuum polarization energy is accounted for by the *interface formalism* that we will introduce below.

The spectrum obtained from H will always be charge conjugation invariant because $\{H, \alpha_3\} = 0$. This invariance implies that the polarized vacuum has zero charge and that the biggest energy gain from a single particle level is m. In contrast, the three-dimensional hedgehog does not have this symmetry, so it can carry a vacuum charge and can have an energy gain as big as $2m$ from a single level.

3.1. Contributions to the quantum energy

The energies of single particle harmonic fluctuations are altered by the interaction with the background, which causes differences in the spectra of H_0 and $H_0 + H_{\text{int}}$. At one loop order the quantum energy is the renormalized sum of these energy differences, which we compute using the spectral method [35]. In this formalism, both isolated bound states (with eigenvalues ϵ_i) and continuum scattering states (with eigenvalues $\sqrt{k^2+m^2}$) contribute to the quantum or *vacuum polarization* energy. The continuum contribution can be expressed as the momentum (k) integral over the product of single particle energies $\omega = \sqrt{k^2+m^2}$ and the change in the density of states for this k, which in turn is related to the momentum derivative of the scattering phase shift $\delta(k)$ [36]. In multi-channel problems, as in Eq. (11), the phase shift reads $\delta(k) = \frac{1}{2i}\ln\det S(k)$, where $S(k)$ is the scattering matrix. For the following general argument we do not make explicit the partial wave decomposition and its degeneracy factor, but details are given below and in Appendix A. As stated above, the trivial dimension z in the string background induces an exponential factor e^{ipz} which in turn changes the dispersion to $\omega = \sqrt{k^2+p^2+m^2}$. Formally, the vacuum polarization energy then becomes

$$\mathcal{E}_q \sim -N_c \int \frac{dp}{2\pi}\left[\int_0^\infty \frac{dk}{2\pi}\sqrt{k^2+p^2+m^2}\,\frac{d}{dk}\delta(k) + \frac{1}{2}\sum_i \sqrt{p^2+\epsilon_i^2}\right], \tag{15}$$

which is still subject to regularization and renormalization. Potential divergences originating from the integral over the momentum p in string direction cancel between the bound state and

continuum contributions due to particular sum rules for scattering data [37,38]. This cancellation allows to integrate over p yielding the vacuum polarization energy per unit length [39]

$$\mathcal{E}_q \sim -\frac{N_c}{4\pi}\left[\int_0^\infty \frac{dk}{2\pi}\sqrt{k^2+m^2}\log\frac{k^2+m^2}{\mu^2}\,\delta(k) - \frac{1}{2}\sum_i\left(\epsilon_i^2\log\frac{\epsilon_i^2+m^2}{\mu^2} - m^2 + \epsilon_i^2\right)\right]. \tag{16}$$

Here μ is an arbitrary scale whose contribution cancels by the same sum rules that rendered the p-integral finite in the first place. It is thus admissible and convenient to choose $\mu = m$. For calculational purposes the phase shift is expressed as the phase of the Jost function, or in the multi-channel case the Jost determinant $F(k) = |F(k)|e^{i\delta(k)}$ [40]. Though k is the real momentum of the scattering states, the Jost function has the important property of being analytic in the upper half complex plane, $\mathrm{Im}(k) \geq 0$. In particular $F(k)$ has simple roots at imaginary momenta representing the bound states. We may thus re-write the integral in Eq. (16) as a contour integral in the complex plane.[3] Since the integrand in the complex plane involves the logarithmic derivative of the Jost function, its simple poles on the imaginary axis account for the bound state contribution, and the only remaining part comes from the discontinuity of the integrand in Eq. (16) along the cut on the imaginary axis, $k = it$ for real $t \geq m$ [35,41]. This produces the spectral integral

$$\mathcal{E}_q \sim -N_c\int_m^\infty \frac{dt}{4\pi}\,t\,u(t) = -N_c\int_0^\infty \frac{d\tau}{4\pi}\,\tau\,u\left(\sqrt{\tau^2+m^2}\right), \tag{17}$$

which, as mentioned above, is a formal result because regularization and renormalization has yet to be implemented. The integrand $u(t)$ is obtained from the Jost function for complex momenta and has the partial wave decomposition

$$u(t) \equiv 2\,u_F(t) = 2\sum_{\ell=-1}^\infty D_\ell\,\nu_\ell(t)\,. \tag{18}$$

In Appendix A we describe in great detail the partial wave decomposition of $\nu_\ell(t)$ and how it is obtained as the logarithm of the Jost determinant from the solutions to the Dirac equation. The degeneracy of the angular momentum channel $\ell \in \{-1, 0, 1, \ldots\}$ is $2D_\ell = 2(2 - \delta_{\ell,-1})$, with the factor of two due to the sum over both Riemann sheets in the relativistic fermion dispersion relation.

As it stands, Eq. (17) is divergent and must be combined with counterterms to obtain a meaningful result. First, we note that the integral in Eq. (17) is rendered finite by subtracting a suitable large t behavior from $\nu_\ell(t)$. The large momentum behavior of scattering data can, however, be estimated from the Volterra integral equation for the wave-function [40] which, by iteration, turns into a series with ascending powers of the background potential, in our case H_{int}. This expansion is known as the Born series, with the first term being the Born approximation. In Appendix A we compute the leading terms of the Born series by iterating the Dirac equation without reference to an integral equation. Hence we obtain a finite integral in Eq. (17) by subtracting sufficiently many leading terms of Born series from its integrand. Of course, we need to add them back, and we do

[3] We refer to Ref. [35] for details on the deformation of the integration contour and how the renormalization procedure also removes the contribution from the semi-circle at infinity.

so in a form which is suitable for renormalization. To identify that suitable form we consider the alternative formulation of the vacuum polarization energy via the functional determinant

$$\mathcal{A} \equiv -TL_z\mathcal{E}_q \sim (-i)\,\ln\det\left(i\partial\!\!\!/ - m - \beta H_{\rm int}\right), \tag{19}$$

which is valid for static configurations. The Feynman series generated via

$$\mathcal{E}^{(n)}_{\rm FD} = \frac{\lambda^n}{n!}\frac{i}{TL_z}\frac{\partial^n}{\partial\lambda^n}\ln\det\left(i\partial\!\!\!/ - m - \lambda\beta H_{\rm int}\right)\big|_{\lambda=0}$$

is also an expansion of $\mathcal{E}_q$ in the interaction strength and thus it is equivalent to the Born series order by order in $H_{\rm int}$. We detail the calculation of the Feynman diagrams, *i.e.* the various orders of the above expansion in Appendix B. These Feynman diagrams are rendered finite when combined with standard counterterms whose contribution to the vacuum polarization energy is $\mathcal{E}_{\rm CT}$. It remains to be observed that for the present model in $D = 3 + 1$ dimensions, the leading four Feynman diagrams are divergent. Hence we need to subtract the four leading terms of the Born series to render the integral in eq. (17) finite:

$$\mathcal{E}_q = -N_c\int_m^\infty \frac{dt}{4\pi}\, t\left[u(t)\right]_4 + \sum_{n=1}^{4}\mathcal{E}^{(n)}_{\rm FD} + \mathcal{E}_{\rm CT}\,. \tag{20}$$

Here and in the following, the notation $[\ldots]_N$ indicates N Born subtractions of scattering data inside the bracket. We stress that both the integral and the combined Feynman-counterterm contribution are individually finite. Thus no further (numerical) cut-off is required.

Even though Feynman diagrams appear in Eq. (20) we emphasize that they only serve as a tool to impose perturbative renormalization conditions within a non-perturbative expression. The whole calculation is of non-perturbative character. This is, for example, established by the fact the Born series, and equivalently the Feynman series, do not capture bound states.

We have already mentioned that (in the numerical simulations) we measure length scales in units of the inverse fermion mass m. From Eqs. (12), (13), (17) and (19) it then follows that measuring the single particle energies and momenta in units of m turns $\mathcal{E}_q$ into a dimensionless number that depends on any of the model parameters only via the counterterm coefficients. Similarly the classical energy has a nontrivial parameter dependence. Yet, the model parameters only enter local contributions to the (total) energy, which are easy to compute. This simplifies considerably the variational scan.

In principle, Eq. (20) could be used directly to compute the vacuum polarization energy. However, the exact calculation of the third- and fourth-order Feynman diagrams (including all finite parts) is very cumbersome. Fortunately, this is not really necessary: since the purpose of the Born subtraction is to render the spectral integral finite, we can subtract *any* function with the correct asymptotic behavior, as long as we can associate this subtraction with a renormalizable Feynman diagram to be added back in. The third- and fourth-order Feynman diagram have a logarithmic divergence, which is also found for a second-order diagram of a simple scalar boson scattering off a background potential. If we adjust the size of this "fake potential" carefully, we can arrange for the logarithmic divergence in the second-order Boson diagram $\mathcal{E}^{(2)}_B$ to match the one from the fermion diagrams $\mathcal{E}^{(3)}_{\rm FD} + \mathcal{E}^{(4)}_{\rm FD}$exactly. Instead of subtracting the third- and fourth- order Born approximation and adding back in the corresponding fermion diagram, we can then subtract the (properly scaled) second Born approximation to a fake boson, and add back in the corresponding second-order boson diagram:

$$\mathcal{E}_q = -N_c \int_m^\infty \frac{dt}{4\pi}\, t \left\{ 2\big[u_F(t)\big]_2 + \frac{\lambda}{N_c}\, u_B^{(2)}(t) \right\} + \mathcal{E}_{F,\mathrm{ren}}^{(1,2)} + \lambda \mathcal{E}_B^{(2)} + \mathcal{E}_{\mathrm{CT}}^{(3,4)} . \tag{21}$$

Note the sign and the missing factor of 2 in the fake boson subtraction, which is due to the bosonic interface formula,[4]

$$\mathcal{E}_B^{(2)} = + \int_m^\infty \frac{dt}{4\pi}\, t\, u_B^{(2)}(t) . \tag{22}$$

Next, we must choose the scaling factor λ (not to be confused with the Higgs coupling in Eq. (1)) such that the logarithmic divergences in the fake boson and fermion diagram match:

$$\lambda \equiv \frac{\big(\mathcal{E}_{\mathrm{FD}}^{(3)} + \mathcal{E}_{\mathrm{FD}}^{(4)}\big)\big|_\infty}{\mathcal{E}_B^{(2)}|_\infty} = \frac{c_F}{c_B} . \tag{23}$$

Here, c_F and c_B are simple radial integrals over the fermion profile functions or the fake boson potential, respectively, which parameterize the logarithmic divergence according to

$$\begin{Bmatrix} \mathcal{E}_{\mathrm{FD}}^{(3)} + \mathcal{E}_{\mathrm{FD}}^{(4)} \\ \mathcal{E}_{\mathrm{B}}^{(2)} \end{Bmatrix} = -i\pi \begin{Bmatrix} c_F \\ c_B \end{Bmatrix} m^{D-4} \int \frac{d^D k}{(2\pi)^D} \frac{1}{(k^2 - m^2 + i\epsilon)^2} + \text{finite} . \tag{24}$$

Explicit formulae for c_F and c_B are listed in Appendices B and C. Even without inspecting these formulae, it is clear that c_F is linear in N_c because it originates from a fermion loop. Hence $\frac{\lambda}{N_c}$ does not depend on N_c.

For the last step, we note that the fermion counterterms for the third- and fourth-order fermion diagram are, within the $\overline{MS}$ scheme, just the negative bare divergence $\mathcal{E}_{CT}^{(3,4)} = -\big(\mathcal{E}_{\mathrm{FD}}^{(3)} + \mathcal{E}_{\mathrm{FD}}^{(4)}\big)\big|_\infty$. Since this has been carefully matched to equal $-\lambda \mathcal{E}_B^{(2)}\big|_\infty$, the last two terms in Eq. (21) combine to the renormalized second-order fake boson diagram in $\overline{MS}$,

$$\lambda \mathcal{E}_B^{(2)} + \mathcal{E}_{CT}^{(3,4)} = \lambda \Big[\mathcal{E}_B^{(2)} - \mathcal{E}_B^{(2)}\big|_\infty \Big] = \lambda\, \mathcal{E}_B^{(2)}|_{\overline{MS}} . \tag{25}$$

Collecting all pieces, we can now rewrite the properly renormalized quantum correction to the energy per unit length of the string background as

$$\begin{aligned} \mathcal{E}_q &= -N_c \int_m^\infty \frac{dt}{4\pi}\, t \left\{ 2\big[u_F(t)\big]_2 + \frac{c_F}{c_B N_c}\, u_B^{(2)}(t) \right\} + \mathcal{E}^{(1,2)}\Big|_{\overline{MS}} + \frac{c_F}{c_B}\, \mathcal{E}_B^{(2)}\Big|_{\overline{MS}} + \Delta\mathcal{E}_{\mathrm{ren}} \\ &= \mathcal{E}_{\mathrm{vac}} + \big[\mathcal{E}_{\mathrm{fermi}}\big]_{\overline{MS}} + \big[\mathcal{E}_{\mathrm{fake}}\big]_{\overline{MS}} + \Delta\mathcal{E}_{\mathrm{ren}} . \end{aligned} \tag{26}$$

We note that simplifying the renormalization calculation by introducing the fake boson subtraction has been repeatedly tested for consistency. For example, in Ref. [22] isospin and gauge symmetries were verified for $\mathcal{E}_q$ even though the individual terms on the right hand side of Eq. (26) are gauge variant. In Eq. (26) we have also added a finite counterterm contribution $\Delta\mathcal{E}_{\mathrm{ren}}$, which arises when we pass from the $\overline{MS}$ scheme to the more physical *on-shell* scheme, such that the renormalized mass parameters agree with the actual physical particle masses. The

[4] We have chosen the background potential in Appendix C to be independent of N_c, so the overall prefactor of N_c is absent.

contribution $\Delta\mathcal{E}_{\rm ren}$ contains the same terms as the classical energy Eq. (9), but has different coefficients computed from the finite parts of the second-order Feynman diagrams,

$$\Delta\mathcal{E}_{\rm ren} = N_c \int_0^\infty dr\, r \left\{ \overline{c}_2 \left[s'(r)^2 + p'(r)^2 + \frac{p(r)^2}{r^2} \right] + \overline{c}_4 \left[1 - s(r)^2 - p(r)^2 \right]^2 \right\}. \tag{27}$$

Details on the coefficients $\overline{c}_2$ and $\overline{c}_4$ are presented in Appendix D. Eq. (26) is the master formula for the quantum energy of a neutral (uncharged) cosmic string. All four contributions are manifestly finite and well suited for numerical evaluation.

3.2. Charged cosmic strings

The quantum fluctuations computed from Eq. (26) usually do not lead to string stabilization. In fact, previous calculations [32,42] for Nielsen–Olesen type configurations showed that, at least for wide profiles, the quantum corrections in $D = 3 + 1$ have the *same* sign as the classical energy. This implies that a stable string does not emerge, even when the quantum part is enhanced by *e.g.* assuming the heavy quark $f \to \infty$ or the large $N_c \to \infty$ limits. Physically, this is not unexpected, as a negative total energy would suggest that the vacuum is *unstable* against cosmic string condensation.

However, individual strings *can* become bound if they manage to attract and bind sufficiently many fermions. In this scenario, fermions explicitly occupy bound states located near the string core, and the complete configuration is *charged*, carrying the quantum number(s) of the trapped fermions. If the charge in question is conserved (at least to the extent that all charge-changing processes are suppressed by a large energy barrier), the charged string becomes (meta-)stable once its total energy is less than the masses of equivalently many free fermions.

More precisely, let $\epsilon_{i,\ell}$ be the eigenvalues of a square-integrable eigenstate of the single particle Hamiltonian, Eq. (11). Their computation is detailed in Appendix E. Such bound states can occur in any angular momentum channel ℓ. As the repulsion of the angular barrier increases with ℓ, the number of bound states decreases and they disappear when ℓ is sufficiently large. We introduce a chemical potential μ and stipulate that all bound states $0 \le \epsilon_{i,\ell} \le \mu \le m$ are occupied explicitly. Emptying any of those levels and filling one that has $\epsilon_{i,\ell} > \mu$ only increases the energy. Assuming a quasi-continuum of states with energy $\sqrt{p^2 + \epsilon_{i,\ell}^2}$ and integrating over the momentum p along the symmetry axis of the string yields the charge per unit length [32]

$$q(\mu) = \frac{N_c}{\pi} \sum_{0 \le \epsilon_{i,\ell} \le \mu} P_{i,\ell}(\mu)\, D_\ell\,, \tag{28}$$

where $P_{i,\ell}(\mu) = \sqrt{\mu^2 - \epsilon_{i,\ell}^2}$ is the Fermi momentum associated to a particular bound state of single particle Hamiltonian, Eq. (11). We have also included the degeneracy $N_c D_\ell$ of each state due to angular momentum and color. As discussed after Eq. (20), the charge per unit length is measured in multiples of m, as are the bound state energies and the chemical potential. Next we invert the relation in Eq. (28) to compute μ_Q, for a prescribed charge per unit length and calculate the binding energy per unit length. In practice this requires three steps:

1. prescribe a value $Q \ge 0$ for the charge per unit length;

2. determine the chemical potential μ_Q by increasing μ in small steps, starting at $\mu = \min_{i,\ell} |\epsilon_{i,\ell}|$, until the condition $q(\mu_Q) = Q$ is met or $\mu > m$ (whence the chosen charge Q cannot be accommodated);
3. Then, sum over all single particle bound states, integrate over p up to the Fermi momentum and subtract $q(\mu_Q)m$, the equivalent energy of free fermions, to obtain the binding energy per unit length [32]

$$\begin{aligned}\mathcal{E}_b(Q) &= N_c \sum_{0\le\epsilon_i\le\mu_Q} \int_0^{P_i(\mu)} \frac{dp_z}{\pi} \left[\sqrt{\epsilon_i^2 + p_z^2} - m\right] D(\epsilon_i) \\ &= \frac{N_c}{2\pi} \sum_{0\le\epsilon_{i,\ell}\le\mu_Q} \left[P_{i,\ell}(\mu_Q)\,(\mu_Q - 2m) + \epsilon_{i,\ell}^2 \ln \frac{P_{i,\ell}(\mu_Q) + \mu_Q}{\epsilon_{i,\ell}}\right] D_\ell\,. \end{aligned} \tag{29}$$

Since $\mathcal{E}_b(Q) < 0$ by construction, charging the string always has a binding effect, though it may not be strong enough to overcome the other contributions to the total energy. In addition, the total number of bound states in a given string background is finite, so that there is a maximal charge per unit length $Q_{\max} = q(m)$ that can be placed on the string, and hence also a limit to the binding effect generated by charging the string.

Equations (26) and (29) comprise all contributions to the quantum energy of a hedgehog type of cosmic string, at least in the limit $N_c \to \infty$ when the fermion determinant dominates all quantum corrections. Since $\mathcal{E}_q$ and $\mathcal{E}_b(Q)$ saturate the $\mathcal{O}(N_c\hbar)$ contribution to the energy, any consideration of $\mathcal{E}_b(Q)$ requires the inclusion of $\mathcal{E}_q$ for consistency.

4. Numerical studies and results

In this section we present the numerical results of our investigation. In the first part, we discuss the individual contributions to the string energy separately, and perform numerical tests on their computation. In the second part we report the results of our variational search for optimal string profile parameters. In all calculations we employ the hedgehog ansatz, Eq. (4) consistent with the boundary conditions derived in Eq. (10). We introduce two variational width parameters w_r and w_a for the background profiles

$$\rho(r) = 1 - a\exp\left(-\frac{r^2}{2w_r^2}\right), \qquad \theta(r) = -\pi\exp\left(-\frac{r}{w_a}\right), \tag{30}$$

of the chiral radius and chiral angle, respectively. The amplitude a describes the decrease in the Higgs condensate at the core of the string: $\rho_0 = 1 - a$. Inspired by the Nielsen–Olesen profiles this amplitude is often chosen as $a = 1$ so that $\rho_0 = 0$. This results in strongly bound states, since fermions located in the vicinity of the string core have near zero mass. Taking $a \to 1$ produces more "shallow" profiles. Though they produce less deeply bound states, a non-zero a may nevertheless be beneficial in reducing the total energy because its smaller gradients decrease the classical energy. The complete ansatz, Eq. (30) thus comprises three variational parameters a, w_r and w_a. The restriction to three variational parameters is, of course, a simplifying approximation as the full back-reaction of the fermion fluctuations on the string profile requires infinitely many such parameters.

Table 1
Contributions to the total energy per unit length for a sample hedgehog string background with parameters $w_a = w_r = 3/m$ and $a = 1$. The model parameters are taken from the physical top quark and Higgs masses: $f = 0.99$ and $\lambda = 0.129$, *cf.* Eqs. (7) and (8). The charge per unit length is set to a typical value of $Q = 5m$.

contribution	comment	equation	depends on	value $[m^2]$
$\mathcal{E}_{\rm cl}$	classical energy	(9)	Yukawa coupling f	14.96
$\mathcal{E}^{(1,2)}_{\rm FD}\vert_{\overline{MS}}$	2nd order fermion diagram	(B.3)	–	−0.13
$\Delta\mathcal{E}_{\rm ren}$	finite counterterm $\overline{MS} \to$ on shell	(D.1)	Yukawa coupling f	0.27
$\mathcal{E}^{(2)}_{\rm B}\vert_{\overline{MS}}$	2nd order fake boson diagram	(C.3)	–	0.02
$\mathcal{E}_{\rm vac}$	vacuum polarization energy	(26)	–	0.94
$\mathcal{E}_b$	charge energy	(29)	string charge Q	−1.85
$\mathcal{E}_{tot}$	total energy per unit length		(f, Q)	14.21

4.1. Numerical details for a single string background

In this section, we survey our numerical procedure for a single background configuration for the case of

$$w_r = w_a = 3/m \qquad \text{and} \qquad a = 1\,. \tag{31}$$

The total energy per unit length of the string background in our framework comprises six contributions, which are listed in Table 1. For a fixed string background, only the classical energy and the finite counterterm (which is always significantly smaller than the classical part) depend on the Yukawa coupling f, since the fermion determinant contribution, $\ln\det\left(i\partial\!\!\!/ - m - \beta H_{\rm int}\right)$, is independent of f when all energies are measured in units of m. Increasing the Yukawa coupling f, *i.e.* the ratio between the fermion mass and the Higgs *vev*, reduces the classical contribution so if the net contribution of the quantum corrections is negative, we can always get a stable string by increasing f to the point where the classical energy penalty becomes negligible. From Table 1, we recognize that this mechanism requires having the string carry charge, since the remaining quantum corrections (*i.e.* the pure fermion determinant) is typically positive and hence does not cause binding. The energy from Eq. (26) may indeed become negative for large Yukawa coupling and very narrow profiles ($w_r, w_a \to 0$) [32]. The Fourier momentum of such profiles then approaches the Landau ghost [43], indicating that the one loop approximation fails. We thus ignore configurations that are afflicted by the Landau ghost problem.

Of all the contributions shown in Table 1, only the vacuum polarization and the charge energy are numerically expensive to compute. The remaining pieces are just simple integrals in coordinate or momentum space. We will now present some numerical details on the computation of these expensive contributions:

Vacuum energy

The main ingredient for the vacuum polarization energy $\mathcal{E}_{\rm vac}$ in Eq. (26) is the sum over the twice Born subtracted logarithm of the Jost function, $D_\ell\,[\nu_\ell(t)]_2$, defined in Eq. (18). Its numerical evaluation is costly because many angular momenta must be included. We present a double logarithmic plot of $D_\ell\,[\nu_\ell(t)]_2$ in Fig. 1. As can be seen, the individual contributions eventually decay with power law ℓ^{-3}, which allows for the use of series accelerators. Still, at least 200 channels, and up to 500 channels at higher momenta, need to be summed to get an accurate estimate of $[u_F(t)]_2$, and likewise for the fake boson contribution $u^{(2)}_B(t)$.

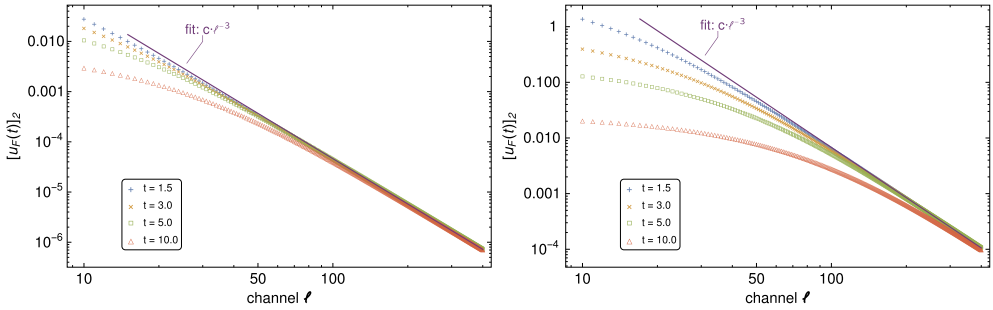

Fig. 1. The contributions to the twice Born subtracted channel sum $u_F(t)$ in eq. (18), for various imaginary momenta t. The left chart corresponds to a narrow string with $w_a = w_r = 2/m$, while the right chart shows the case of a wide string with $w_a = w_r = 7/m$. As can be seen, wider strings generally require more channels to reach the asymptotic region with a power law decay. Also, the shift of the asymptotic region to larger channels with increasing momentum is much more pronounced for wider strings.

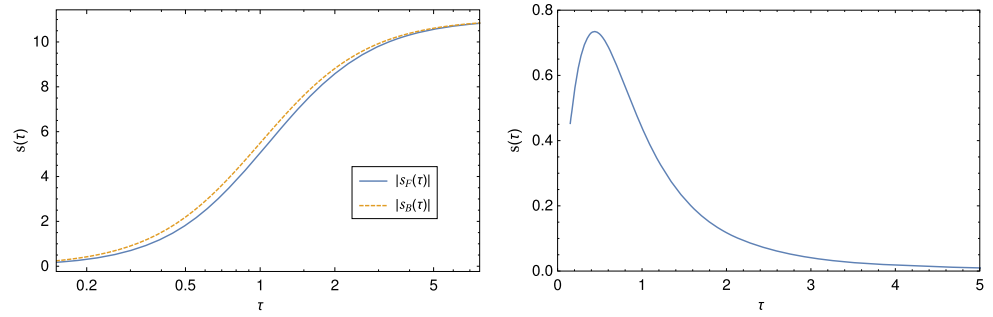

Fig. 2. *Left*: The fermionic and fake boson contributions to the integrand eq. (32) for the vacuum polarization energy. For clarity, the contribution is multiplied by τ to emphasize the asymptotic decay $\sim 1/\tau$. *Right:* The full integrand $s(\tau)$ eq. (32) for the vacuum energy.

In order to further analyze the vacuum energy, we separate the integrand in $\mathcal{E}_{\rm vac}$ into the fermion and fake boson parts,

$$s_F(\tau) \equiv -\frac{N_c}{4\pi}\,\tau\,\left[2u_F(\sqrt{\tau^2+m^2})\right]_2\,,$$
$$s_B(\tau) \equiv +\frac{N_c}{4\pi}\,\tau\,\frac{c_F}{c_B N_c}\,u_B^{(2)}(\sqrt{\tau^2+m^2})\,, \tag{32}$$

where we have also changed the momentum variable $t \to \tau \equiv \sqrt{t^2-m^2}$. Here, each function $u(t)$ is the sum of the logarithmic Jost function over all angular momenta, *cf.* Eqs. (18) and (C.5).

The fake boson method relies on the fact that a properly rescaled second-order boson contribution possesses the same logarithmic divergence as the third- and fourth-order Feynman diagrams, *i.e.* the large-momenta behavior of the two integrands $s_F(\tau)$ and $s_B(\tau)$ in Eq. (32) must match. In the left panel of Fig. 2, we present the products $\tau\, s_F(\tau)$ and $\tau\, s_B(\tau)$, because they should asymptotically approach the (same) constant in order to cancel the (same) logarithmic divergence in $\mathcal{E}_{\rm vac}$. This is indeed the case to a very high accuracy. Though the full calculation is computationally expensive, it has the advantage to provide an independent test for the precision of our numerics.

Table 2
Energies and angular momenta of the fermion bound states in the background of the hedgehog soliton with $w_a = w_r = 3/m$ and $a = 1$.

channel index ℓ	# bound states	positive bound state energies $[m]$
-1	14	0.133, 0.601, 0.702, 0.807, 0.903, 0.930, 0.970
0	10	0.427, 0.616, 0.807, 0.866, 0.996
1	8	0.672, 0.859, 0.957, 0.973
2	2	0.862
> 2	0	–

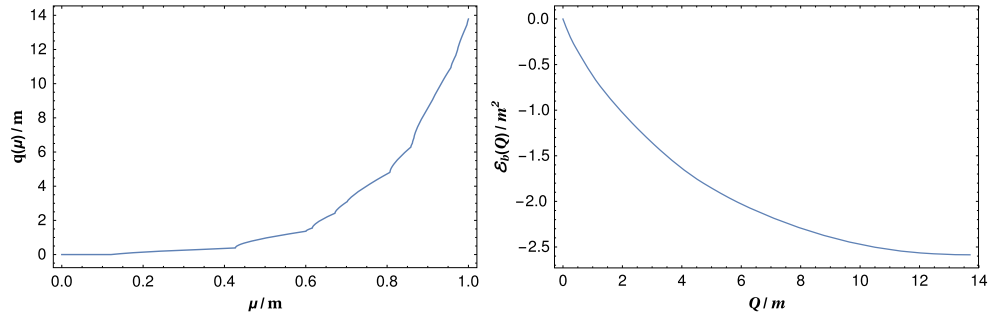

Fig. 3. *Left*: The charge per unit length $q(\mu)$ induced on the hedgehog string by filling all levels lower than a chemical potential μ, for the string background with $w_a = w_r = 3/m$. *Right*: The binding energy $\mathcal{E}_b(Q)$ due to a prescribed charge per unit length Q, for the same string background.

In the right panel of Fig. 2, we show the complete integrand $s(\tau) \equiv s_F(\tau) - s_B(\tau)$ of the integral in $\mathcal{E}_{\text{vac}}$. With the fake boson subtraction, the integrand vanishes very quickly already for moderate momenta, which allows for an accurate evaluation[5] of $\mathcal{E}_{\text{vac}} \approx 0.94m^2$, as listed in Table 1.

Bound state energy

We compute matrix elements of the Hamiltonian $H = H_0 + H_{\text{int}}$, Eqs. (12) and (13) with respect to the eigenfunctions of H_0. The details of this calculation are described in Appendix E. The would-be scattering and shallow bound states near threshold will still vary considerably with the artificial numerical parameters; but the real bound-state spectrum of eigenvalues $< 0.95m$ is stable. In Table 2, we list the positive bound states for all angular momentum channels for the string background with $w_a = w_r = 3/m$. As discussed above, the interaction is charge conjugation invariant, so for each positive energy solution there is a negative one.

With the bound states at hand, we can evaluate the binding effect from charging the string as laid out in section 3.2. Here we first report the maximal charge (per unit length) which the string with the parameters from Eq. (31) can accommodate. It is obtained by equating the chemical potential with the fermion mass in Eq. (28): $q(m) = 13.78m$.

[5] We truncate the τ-integral at a very small and a very large cutoffs and estimate the remainder in both regions by fits to the integrand which are then extrapolated and integrated analytically. At small τ, we use a quadratic polynomial fit, while at large momenta $\tau \gg 1$, we assume a power-law decay. The cutoffs are determined such that the low- and high-momentum extrapolations are less than 5% of the bulk contribution. Stability of this procedure against moderate variations of the cutoffs was verified.

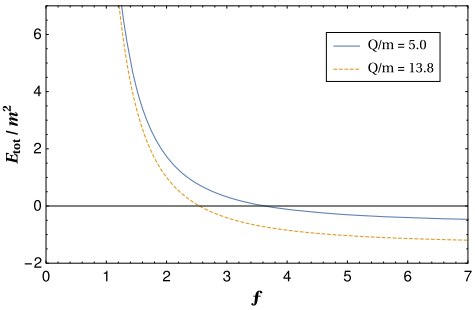

Fig. 4. The total energy per unit length, Eq. (33) of a cosmic string background with widths $w_a = w_r = 3/m$ as a function of the Yukawa coupling at fixed charge per unit length.

Secondly, we plot the charge, Eq. (28), as function of the chemical potential in Fig. 3. It is monotonically increasing by construction and can be inverted numerically to yield the chemical potential $\mu(Q)$ necessary to produce a given charge Q. With this relation, the energy per unit length $\mathcal{E}_b(Q)$ induced by the string charge Q can be evaluated from Eq. (29). For our model string, Eq. (31), $\mathcal{E}_b(Q)$ is plotted in the right panel of Fig. 3. By construction, $\mathcal{E}_b(Q)$ is negative and monotonically decreasing up to the maximal charge $q(m)$ allowed by the Pauli principle. Fig. 3 shows that the binding energy due to a maximally charged string is $\mathcal{E}_b(q(m)) = -2.5\,m^2$, while a realistic value for a moderate charge $Q \approx 5m$ is $\mathcal{E}_b(Q) = -1.85\,m^2$.

Total energy

Comparing the binding effect of charging the string with the remaining contributions to the string energy in Table 1, obviously shows that the charged string with $w_a = w_r = 3/m$ is *not* stable when the Yukawa coupling f is adjusted to the physical top quark mass. A slight increase of f to reduce the large classical energy as in Fig. 1 indeed gives a bound object. In Fig. 4, we show the total energy per unit length

$$E_{\text{tot}}(Q) = \mathcal{E}_{\text{cl}} + \mathcal{E}_q + \mathcal{E}_b(Q) \tag{33}$$

of a charged string with variational parameters $w_a = w_r = 3/m$ as a function of the Yukawa coupling f. For a moderate charge, $Q = 5\,m$, the string becomes bound around $f \approx 3.66$, which corresponds to a fermion mass of $m = 637$ GeV (assuming the empirical *vev*, $v = 174$ GeV). If instead we allow the string to be maximally charged, the threshold for binding drops to $f \approx 2.55$ corresponding to a fermion mass of $m = 443$ GeV.

4.2. *Variational searches for bound cosmic strings*

The results for the single configuration presented above are representative for a typical string background. They give an upper limit on the fermion mass needed to bind a (charged) cosmic string. We can improve this limit by varying the variational parameters of the background profile to identify the optimal string shape for any given coupling or charge. For this purpose, we have varied the width parameters w_a and w_r in the string profile eq. (30) within the range $w_a, w_r \in [1/m, 10/m]$. Smaller values may yield a lower $\mathcal{E}_b$ as an artifact of the Landau pole and are therefore discarded. In addition to testing (several hundred) configurations that all have a vanishing Higgs background at the string core, we have also included about 30 "shallow" configurations with amplitude parameter $a \in [0.1,\ 0.9]$ in the set of sample string profiles. For each

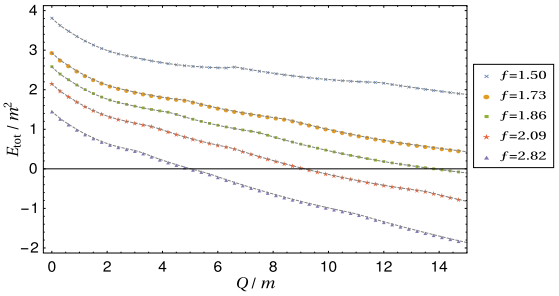

Fig. 5. The total energy per unit length of the optimal string configuration, as a function of the string charge per unit length, Q, and for various values of the Yukawa coupling f.

of these configurations we have computed the vacuum polarization energy and the bound state spectrum. We then select a value for the Yukawa coupling f and compute the total binding energy $E_{\rm tot}(Q)$, Eq. (33) as a function of Q, the string charge per unit length, for all configurations. Finally, at any given Q we determine the minimal $E_{\rm tot}(Q)$. In Fig. 5, we show the final result of this variational search. Typically a particular configuration is optimal for a finite interval in Q. When Q is increased eventually the maximal charge $q(m)$ that this configuration can accommodate is reached and a switch occurs to another optimal configuration that can hold a larger charge. This switching of optimal configurations gives rise to small bends in the curves. For small Yukawa couplings, the total binding energy stays positive and no stable string is found. As we increase the Yukawa coupling, the total binding energy decreases for large Q and eventually turns negative. We find that the smallest Yukawa coupling, for which a stable charged string is observed is $f \approx 1.86$. This corresponds to a quark mass of $m \approx 324$ GeV. This binding occurs at an almost maximal charge per unit length of $Q \approx 13\,m$. As we further increase the Yukawa coupling, less and less charge is necessary to obtain a bound string. At $f \approx 2.82$ or a quark mass of $m \approx 490$ GeV, a relatively moderate charge of $Q \approx 5\,m$ is sufficient to bind the cosmic string.

We find four general features of the optimal string configuration:

1. All optimal configurations have $a = 1$, *i.e.* it is preferable to have the Higgs field vanish at the origin, as in the Nielsen–Olesen profile. This is somewhat unexpected as it contrasts with the motivation for the hedgehog configuration, Eq. (2). The profiles with $a = 1$ have fewer, but deeper bound states and a considerable classical energy. The "shallow" configurations with a non-vanishing Higgs condensate at the string core are not optimal, even though they cost less classical energy to form. Since for shallow configurations all bound states are close to threshold, the loss in binding energy at large charges outweighs the gain in classical energy.
2. All optimal configurations have $w_a = 2m$, *i.e.* the angular twisting of the Higgs emerges close to the string core, even when the radial distribution of the string profile is rather wide.[6]
3. The width of the radial Higgs profile generally increases with increasing charge Q, as can be seen from Fig. 6. Since wider strings bind charge more easily, the optimal configurations are fairly wide for the lightest possible quarks masses. However, we have included radial

[6] We have also investigated configurations with smaller $w_a = 1.1m$ and $w_a = 1.5m$, which were not optimal, so that the value $w_a = 2m$ is not a corner case.

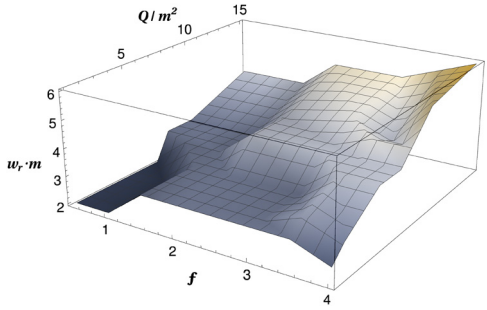

Fig. 6. The radial width w_r of the optimal string configuration (in units of m^{-1}) for various charges and Yukawa couplings at a fixed angular width $w_a = 2/m$.

widths up to $w_r = 10/m$ in our variational search, and extremely wide configurations with $w_r \geq 7/m$ are not preferable.

4. For $f > 1.86$, we find bound strings at a critical charge $Q > Q^*$, which *decreases* with increasing quark mass. At the same time, the radial width of the chiral radius of the optimal configuration for the critical charge Q^* actually decreases for higher fermion masses, *e.g.* from $w_r^* = 4.0/m$ at $f = 1.86$ to $w_r^* = 1.90/m$ at $f = 5.0$.

5. Summary and conclusions

We have investigated the dynamical stabilization of a cosmic string in an $SU(2)$ gauge theory that is a slightly reduced version of the electroweak standard model. The string configuration itself consists of a twisted string-like deviation from the Higgs *vev* without any gauge field admixture, *i.e.* a thin line defect carved into the Higgs condensate. This ansatz is inspired by the well-known hedgehog ansatz for the chiral soliton in quark models. In contrast to the Nielsen–Olesen configuration, the present one is characterized by two profile functions for the Higgs field, a chiral radius and a chiral angle. The latter is similar to the Skyrme model solution. Classically, the string configuration is not stable, but it tends to attract fermions which may be bound in the vicinity of the string core to produce a *charged* string. As a consequence the charged string becomes stable if the quark mass is large enough. For consistency of the $\hbar$ expansion we must also include the contribution of the scattering states to the quantum energy, and renormalize conventionally to make contact with empirical model parameters. This is the most complicated and numerically expensive part of the calculation.

We find that at a fairly large charge the string becomes bound when the fermion mass exceeds a value of about 320 GeV. By charge conservation it can only decay into a system of equally many free fermions which, however, has a bigger energy. The resulting string profiles are characterized by a fairly narrow chiral angle that has a width of about $w_a = 2/m$ while the chiral radius is more extended with a width $w_r = 4/m$. To put this in perspective, consider the optimal string at the smallest possible fermion mass of 320 GeV. If it extends over a length equal to the diameter of the sun, the mass of the optimal string would only be a fraction (10^{-20}) of the sun's mass, however all concentrated in a thin filament with a thickness of less than 0.004 fm.

The results presented here are qualitatively similar to those from previous investigations that instead of featuring a twisted Higgs field allowed for a non-trivial gauge-field admixture in the cosmic string [32] as variants of the Nielsen–Olesen configuration [23]; the gauge field component of the optimal configuration turned out to be marginal. In fact, the presently obtained

fermion mass and charges necessary to stabilize a string are only about 10% larger than those in the previous study. This indicates that the dominant mechanism in the binding of the cosmic string, *i.e.* the attraction of fermions, is mainly due to the small Higgs *vev* seen by fermions that are strongly bound in the vicinity of the string. Complicated gauge field additions or topological windings play, apparently, a minor role.

The results presented in this work are interesting in their own right, as they show that a potential fourth generation of heavy quarks (with masses $m > 320\,\mathrm{GeV}$) that couple to the Higgs condensate in the standard way can exist neither today nor in the early universe (in sufficient numbers) without causing the generation of stable cosmic strings that eventually form networks. Such networks would be detectable *e.g.* by their gravitational lensing or their distortion of the cosmic microwave background, and can therefore be ruled out by experiment. Although our reasoning was made in a simplified version of the standard model, we believe that the qualitative effect carries over to the full electroweak theory since enlarging the variational space can only lower the energy.

The simplified configuration of a bound string achieved in the present work allows to study extended networks of realistic cosmic strings in a more accessible framework in which fermions couple to a prescribed Higgs background without dynamical gauge fields.

Nevertheless, the hedgehog string configuration for the Higgs field can be augmented by a gauge field component. Adopting Weyl gauge the decomposition of a possible hedgehog gauge field must have the same structure as $\Phi^\dagger \nabla \Phi$ from Eq. (2),

$$\boldsymbol{W}(\boldsymbol{r}) = \hat{\boldsymbol{r}} \begin{pmatrix} A(r) & i\mathrm{e}^{i\varphi} B(r) \\ i\mathrm{e}^{-i\varphi} B(r) & A(r) \end{pmatrix} + \frac{i}{r} \hat{\boldsymbol{\varphi}} \begin{pmatrix} a(r) & -i\mathrm{e}^{i\varphi} b(r) \\ i\mathrm{e}^{i\varphi} b(r) & -a(r) \end{pmatrix}, \tag{34}$$

which introduces up to four additional radial functions in the plane perpendicular to the string; all of which vanish asymptotically. Of course, this expands the variational computation significantly. As a first simplification, the Higgs configuration would be fixed at the optimal configuration established in the current study.

Acknowledgements

N. G. is supported in part by the NSF through grant PHY-1520293. H. W. is supported in part by the NRF (South Africa) by grant 109497.

Appendix A. Scattering off a hedgehog type of string

We solve the multi-channel scattering problem of a Dirac fermion in $D = 2 + 1$ dimensions subject to the single particle Hamiltonian, Eq. (11). We employ planar polar coordinates (r, φ) and perform a partial wave decomposition. Since neither the z-component of the total angular momentum $J_z = L_z + S_z$ nor isospin I_z are separately conserved, we label the solutions of the free Dirac equation by the eigenvalue $G \in \mathbb{Z}$ of the *grand spin* operator $G_z = J_z + I_z$. The quantum number $\ell \in \mathbb{Z}$ of L_z is determined by the angular dependency $e^{i\ell\varphi}$. For each value of ℓ there are four solutions of the free Dirac equation with given energy ϵ (and 4 solutions with energy $-\epsilon$ related by charge conjugation). These degenerate solutions do not all have the same angular dependence, since the free Hamiltonian contains φ-dependent terms and ℓ is not a good quantum number. However, we can still use it as an angular momentum *channel index* in the partial wave decomposition. The actual angular dependence of the four degenerate solutions to the free Dirac equation is

$$\begin{aligned}
\langle\varphi|(\ell+1)++\rangle &= e^{i(\ell+1)\varphi}\begin{pmatrix}1\\0\end{pmatrix}_S\otimes\begin{pmatrix}1\\0\end{pmatrix}_I\\
\langle\varphi|\ell+-\rangle &= (-i)e^{i\ell\varphi}\begin{pmatrix}1\\0\end{pmatrix}_S\otimes\begin{pmatrix}0\\1\end{pmatrix}_I\\
\langle\varphi|(\ell+2)-+\rangle &= i\,e^{i(\ell+2)\varphi}\begin{pmatrix}0\\1\end{pmatrix}_S\otimes\begin{pmatrix}1\\0\end{pmatrix}_I\\
\langle\varphi|(\ell+1)--\rangle &= e^{i(\ell+1)\varphi}\begin{pmatrix}0\\1\end{pmatrix}_S\otimes\begin{pmatrix}0\\1\end{pmatrix}_I .
\end{aligned}\tag{A.1}$$

The subscripts S and I indicate that the corresponding two-component spinors dwell in spin and isospin spaces, respectively. Each of these solutions is then considered as a four-component angular spinor. These states have grand spin $G=\ell$ or $G=\ell+2$, respectively, and this quantum number is conserved by the free Hamiltonian. The channel index $\ell\in\mathbb{Z}$ is signed, but channels ℓ and $-(\ell+2)$ are related by symmetry, so that we can restrict $\ell=-1,0,1,2,\ldots$ with degeneracy $D_\ell=2-\delta_{\ell,-1}$.

From the set of spinors in Eq. (A.1) we always combine those with equal grand spin and dress them by radial functions to establish the basis of the partial wave decomposition,

$$\begin{aligned}
\psi_1(r,\varphi) &= \begin{pmatrix} f_1(r)\langle\varphi|(\ell+1)++\rangle\\ g_1(r)\langle\varphi|(\ell+2)-+\rangle\end{pmatrix} && G=\ell+2\\
\psi_2(r,\varphi) &= \begin{pmatrix} f_2(r)\langle\varphi|(\ell+0)+-\rangle\\ g_2(r)\langle\varphi|(\ell+1)--\rangle\end{pmatrix} && G=\ell\\
\psi_3(r,\varphi) &= \begin{pmatrix} f_3(r)\langle\varphi|(\ell+2)-+\rangle\\ g_3(r)\langle\varphi|(\ell+1)++\rangle\end{pmatrix} && G=\ell+2\\
\psi_4(r,\varphi) &= \begin{pmatrix} f_4(r)\langle\varphi|(\ell+1)--\rangle\\ g_4(r)\langle\varphi|(\ell+0)+-\rangle\end{pmatrix} && G=\ell\,.
\end{aligned}\tag{A.2}$$

Each of these eight-component spinors is a regular solution to the free Dirac equation when

$$f_i^{(0)}(r)=J_\alpha(kr)\qquad\text{and}\qquad g_i^{(0)}(r)=\frac{\epsilon-m}{k}\,J_\beta(kr)\,,\tag{A.3}$$

where $|\epsilon|\geq m$ with $k=\sqrt{\epsilon^2-m^2}>0$. The order of the Bessel function is determined by the angular momentum associated with radial function, *i.e.* for $i=3$ we have $\alpha=\ell+2$ and $\beta=\ell+1$.

When the interaction H_{int} in Eq. (13) is switched on, the radial functions differ from the free case eq. (A.3) and mix among each other. To compactly formulate the resulting scattering problem we define two-component objects

$$\vec{u}(r)=\begin{pmatrix}f_1(r)\\f_4(r)\end{pmatrix},\quad \vec{v}(r)=\begin{pmatrix}g_1(r)\\g_4(r)\end{pmatrix},\quad \vec{w}(r)=\begin{pmatrix}f_2(r)\\f_3(r)\end{pmatrix}\quad\text{and}\quad \vec{h}(r)=\begin{pmatrix}g_2(r)\\g_3(r)\end{pmatrix}.\tag{A.4}$$

The Dirac equation reduces to two sets of ordinary differential equations (ODE)

$$\begin{aligned}
(\epsilon-m)\,\vec{u} &= \mathbf{D}\cdot\vec{v}-\mathbf{X}\cdot\vec{u}+\mathbf{Y}\cdot\vec{v}\\
(\epsilon+m)\,\vec{v} &= \overline{\mathbf{D}}\cdot\vec{u}+\mathbf{X}\cdot\vec{v}-\mathbf{Y}\cdot\vec{u}
\end{aligned}\tag{A.5}$$

for $\vec{u}$ and $\vec{v}$ and

$$\begin{aligned}(\epsilon - m)\,\vec{w} &= \widehat{\mathbf{D}} \cdot \vec{h} - \mathbf{X} \cdot \vec{w} - \mathbf{Y} \cdot \vec{h} \\ (\epsilon + m)\,\vec{h} &= \widehat{\overline{\mathbf{D}}} \cdot \vec{w} + \mathbf{X} \cdot \vec{h} + \mathbf{Y} \cdot \vec{w}\end{aligned} \tag{A.6}$$

for $\vec{w}$ and $\vec{h}$. The separation into two decoupled sets is a feature of the hedgehog configuration, Eq. (2) and does not occur when gauge fields are included [32]. The boldface objects are 2×2 matrix operators. The radial derivatives and the centrifugal barriers are combined in the diagonal matrices

$$\mathbf{D} = \operatorname{diag}\left(\frac{\ell+2}{r} + \partial_r\,,\ \frac{\ell}{r} - \partial_r\right) \qquad \overline{\mathbf{D}} = \operatorname{diag}\left(\frac{\ell+1}{r} - \partial_r\,,\ \frac{\ell+1}{r} + \partial_r\right) \tag{A.7}$$

$$\widehat{\mathbf{D}} = \operatorname{diag}\left(\frac{\ell+1}{r} + \partial_r\,,\ \frac{\ell+1}{r} - \partial_r\right) \qquad \widehat{\overline{\mathbf{D}}} = \operatorname{diag}\left(\frac{\ell}{r} - \partial_r\,,\ \frac{\ell+2}{r} + \partial_r\right). \tag{A.8}$$

The interaction matrices are expressed in terms of the profile functions in Eq. (5),

$$\mathbf{X} = m\begin{pmatrix} 1 - s(r) & 0 \\ 0 & 1 - s(r) \end{pmatrix} \qquad \mathbf{Y} = m\begin{pmatrix} 0 & p(r) \\ -p(r) & 0 \end{pmatrix}. \tag{A.9}$$

For given energy $|\epsilon| > m$ and angular momentum ℓ we identify outgoing free polar waves, which are parameterized by Hankel functions of the first kind $H_\nu^{(1)}(kr)$. We concentrate on the system Eq. (A.5); the second system Eq. (A.6) can be treated analogously. In the free case, the two linear independent complex polar wave solutions for $\vec{u}^{\,(0)}$ and $\vec{v}^{\,(0)}$ can be conveniently placed into the columns of two 2×2 matrices,

$$\mathcal{H}_u = \operatorname{diag}\Big(H_{\ell+1}^{(1)}(kr),\ H_{\ell+1}^{(1)}(kr)\Big) \qquad \text{and} \qquad \mathcal{H}_v = \kappa \operatorname{diag}\Big(H_{\ell+2}^{(1)}(kr),\ H_{\ell}^{(1)}(kr)\Big), \tag{A.10}$$

where

$$\kappa = \frac{k}{\epsilon + m} = \frac{\epsilon - m}{k}. \tag{A.11}$$

It is important to parameterize κ as an odd function of k because although $\kappa = \sqrt{\frac{\epsilon-m}{\epsilon+m}}$ is correct for $k \geq 0$, it is deceptive for analytic continuation. Similarly we put the two linearly independent solutions of the full ODE system (A.5) for $\vec{u} = (f_1, f_4)$ and $\vec{v} = (g_1, g_4)$ into the columns of 2×2 matrices

$$\mathbf{U} = \Big(\vec{u}^{\,(1)}(r),\ \vec{u}^{\,(2)}(r)\Big) \qquad \text{and} \qquad \mathbf{V} = \Big(\vec{v}^{\,(1)}(r),\ \vec{v}^{\,(2)}(r)\Big), \tag{A.12}$$

respectively. It is convenient to factor out the free part and define

$$\mathbf{U} = \mathcal{F} \cdot \mathcal{H}_u \qquad \mathbf{V} = \mathcal{G} \cdot \mathcal{H}_v\,, \tag{A.13}$$

where the new Jost matrices obey the boundary conditions

$$\lim_{r\to\infty} \mathcal{F}(r) = \lim_{r\to\infty} \mathcal{G}(r) = \mathbb{1}\,. \tag{A.14}$$

Inserting these ansätze Eq. (A.5) yields the following equations for the 2×2 Jost matrices

$$\partial_r \mathcal{F} = \Big[\mathbf{\Lambda}_F - \mathbf{CY}\Big]\mathcal{F} + \mathcal{F}\Big[+k\,\mathbf{C}\,\mathbf{Z}_F - \mathbf{\Lambda}_F\Big] + \Big[-k\,\mathbf{C} + \kappa\,\mathbf{CX}\Big]\mathcal{G}\,\mathbf{Z}_F$$
$$\partial_r \mathcal{G} = \Big[\mathbf{\Lambda}_G - \mathbf{CY}\Big]\mathcal{G} + \mathcal{G}\Big[-k\,\mathbf{C}\,\mathbf{Z}_G - \mathbf{\Lambda}_G\Big] + \Big[+k\,\mathbf{C} + \frac{1}{\kappa}\,\mathbf{CX}\Big]\mathcal{F}\,\mathbf{Z}_G\,. \tag{A.15}$$

Here, the 2×2 matrix $\mathbf{C} = \mathrm{diag}(1,-1)$ inverts the sign of the lower component. The Hankel functions and centrifugal terms, which are of kinematic origin, enter through the matrices

$$\mathbf{Z}_F = \mathrm{diag}\left(\frac{H^{(1)}_{\ell+2}(kr)}{H^{(1)}_{\ell+1}(kr)}\,,\ \frac{H^{(1)}_{\ell}(kr)}{H^{(1)}_{\ell+1}(kr)}\right), \qquad \mathbf{Z}_G = \mathrm{diag}\left(\frac{H^{(1)}_{\ell+1}(kr)}{H^{(1)}_{\ell+2}(kr)}\,,\ \frac{H^{(1)}_{\ell+1}(kr)}{H^{(1)}_{\ell}(kr)}\right),$$
$$\mathbf{\Lambda}_F = \frac{1}{r}\,\mathrm{diag}\,(\ell+1\,,\,-(\ell+1))\,, \qquad \mathbf{\Lambda}_G = \frac{1}{r}\,\mathrm{diag}\,(-(\ell+2)\,,\,\ell)\,. \tag{A.16}$$

We observe that asymptotically, *i.e.* $r\to\infty$, the first columns of $\mathbf{U}$ and $\mathbf{V}$ correspond to an outgoing wave only in the channel ψ_1 while the second columns have an outgoing wave only in the channel ψ_4. Finally noting that the complex conjugate of the Jost solution also solves the (real) radial ODE system the scattering wave function is the linear combination

$$\Psi_u = \mathcal{F}^*\cdot\mathcal{H}^*_u + \mathcal{F}\cdot\mathcal{H}_u\cdot\mathcal{S}\,. \tag{A.17}$$

The S-matrix is determined by the requirement that Ψ_u is regular at the origin $r\to 0$, with the result

$$\mathcal{S} = -\lim_{r\to 0}\mathcal{H}_u^{-1}\cdot\mathcal{F}^{-1}\cdot\mathcal{F}^*\cdot\mathcal{H}^*_u = -\lim_{r\to 0}\mathcal{H}_v^{-1}\cdot\mathcal{G}^{-1}\cdot\mathcal{G}^*\cdot\mathcal{H}^*_v\,. \tag{A.18}$$

As mentioned in the main text, it is advantageous to find the Jost matrix for momenta analytically continued to the imaginary axis, $k\to it$ with $t>0$, since the resulting spectral integral, Eq. (17) fully accounts for the bound state contribution to $\mathcal{E}_q$. The continuation must, in principle, be carried out separately for both signs of the energy $\epsilon = \pm\sqrt{m^2+k^2}$. In the present case, the theory is charge-conjugation invariant for real momenta and we can select one sign of the energy (say, $\epsilon>0$). The second Riemann sheet then contributes an overall factor of two to the vacuum energy per unit length, *cf.* Eq. (21). For simplicity, we only present the derivation for Eq. (A.5); the corresponding results for Eq. (A.6) can be obtained by some simple sign changes and angular momentum relabelings.

If we assume that the Jost matrices $\mathcal{F}$ and $\mathcal{G}$, Eq. (A.15) are analytic functions of the momentum, the continuation $k\to it$ yields

$$\partial_r \mathcal{F} = \Big[\mathbf{\Lambda}_F - \mathbf{CY}\Big]\mathcal{F} + \mathcal{F}\Big[t\,\mathbf{C}\,\mathscr{Z}_F - \mathbf{\Lambda}_F\Big] + \Big[-t\,\mathbf{C} + z_k^*\,\mathbf{CX}\Big]\mathcal{G}\,\mathscr{Z}_F$$
$$\partial_r \mathcal{G} = \Big[\mathbf{\Lambda}_G - \mathbf{CY}\Big]\mathcal{G} + \mathcal{G}\Big[-t\,\mathbf{C}\,\mathscr{Z}_G - \mathbf{\Lambda}_G\Big] + \Big[t\,\mathbf{C} - z_k\,\mathbf{CX}\Big]\mathcal{F}\,\mathscr{Z}_G\,. \tag{A.19}$$

Here, $\mathcal{F}=\mathcal{F}(it,r)$ and $\mathcal{G}=\mathcal{G}(it,r)$ are again complex 2×2 matrices. The kinematical factor κ from Eq. (A.11) has turned into a pure phase

$$\kappa \xrightarrow{k\to it} i\,z_k^*\,, \qquad z_k = \frac{m+i\sqrt{t^2-m^2}}{t} = \frac{1}{z_k^*} \tag{A.20}$$

and the Hankel functions are replaced by modified Bessel functions contained in

$$\mathscr{Z}_F \equiv i\mathbf{Z}_F(itr) = \mathrm{diag}\left(\frac{K_{\ell+2}(tr)}{K_{\ell+1}(tr)}\,,\ -\frac{K_{\ell}(tr)}{K_{\ell+1}(tr)}\right)$$
$$\mathscr{Z}_G \equiv i\mathbf{Z}_G(itr) = \mathrm{diag}\left(-\frac{K_{\ell+1}(tr)}{K_{\ell+2}(tr)}\,,\ \frac{K_{\ell+1}(tr)}{K_{\ell}(tr)}\right). \tag{A.21}$$

The Born series is obtained by expanding these differential equations in powers of the interaction. The leading term is always the 2×2 unit matrix, so that $\mathcal{F} = \mathbb{1} + \mathcal{F}_1 + \mathcal{F}_2 + \ldots$ and $\mathcal{G} = \mathbb{1} + \mathcal{G}_1 + \mathcal{G}_2 + \ldots$. This expansion leads to

$$\begin{aligned}
\partial_r \mathcal{F}_1 &= \left[\mathbf{\Lambda}_F\,,\,\mathcal{F}_1\right] + t\left(\mathcal{F}_1\,\mathbf{C} - \mathbf{C}\,\mathcal{G}_1\right)\mathscr{Z}_F + z_k^*\,\mathbf{CX}\,\mathscr{Z}_F - \mathbf{CY} \\
\partial_r \mathcal{G}_1 &= \left[\mathbf{\Lambda}_G\,,\,\mathcal{G}_1\right] + t\left(\mathbf{C}\,\mathcal{F}_1 - \mathcal{G}_1\,\mathbf{C}\right)\mathscr{Z}_G - z_k\,\mathbf{CX}\,\mathscr{Z}_G - \mathbf{CY} \\
\partial_r \mathcal{F}_2 &= \left[\mathbf{\Lambda}_F\,,\,\mathcal{F}_2\right] + t\left(\mathcal{F}_2\,\mathbf{C} - \mathbf{C}\,\mathcal{G}_2\right)\mathscr{Z}_F + z_k^*\,\mathbf{CX}\,\mathcal{G}_1\,\mathscr{Z}_F - \mathbf{CY}\,\mathcal{F}_1 \\
\partial_r \mathcal{G}_2 &= \left[\mathbf{\Lambda}_G\,,\,\mathcal{G}_2\right] + t\left(\mathbf{C}\,\mathcal{F}_2 - \mathcal{G}_2\,\mathbf{C}\right)\mathscr{Z}_G - z_k\,\mathbf{CX}\,\mathcal{F}_1\,\mathscr{Z}_G - \mathbf{CY}\,\mathcal{G}_1\,.
\end{aligned} \tag{A.22}$$

For the quantum energy we require the logarithmic Jost functions $\widetilde{\nu}(t)$ defined by

$$\exp\left[\widetilde{\nu}_F(t)\right] = \lim_{r\to 0} \det \mathcal{F}(it, r) \qquad \text{and} \qquad \exp\left[\widetilde{\nu}_G(t)\right] = \lim_{r\to 0} \det \mathcal{G}(it, r)\,. \tag{A.23}$$

These quantities have the Born expansion

$$\begin{aligned}
\widetilde{\nu}_F(t) &= \operatorname{tr}\mathcal{F}_1 + \operatorname{tr}\left(\mathcal{F}_2 - \frac{1}{2}\,\mathcal{F}_1\cdot\mathcal{F}_1\right) + \cdots \equiv \widetilde{\nu}_F^{(1)}(t) + \widetilde{\nu}_F^{(2)}(t) + \cdots \\
\widetilde{\nu}_G(t) &= \operatorname{tr}\mathcal{G}_1 + \operatorname{tr}\left(\mathcal{G}_2 - \frac{1}{2}\,\mathcal{G}_1\cdot\mathcal{G}_1\right) + \cdots \equiv \widetilde{\nu}_G^{(1)}(t) + \widetilde{\nu}_G^{(2)}(t) + \cdots\,.
\end{aligned} \tag{A.24}$$

To find the relationship between $\widetilde{\nu}_F(t)$ and $\widetilde{\nu}_G(t)$ and, most importantly $\nu(t) = \nu_\ell(t)$ that enters Eq. (18), we recall that the Jost function is defined by the Wronskian between the Jost solution and the *regular* solution. The latter is defined by a momentum-independent boundary condition at the origin $r \to 0$. As $r \to 0$ the Higgs field does not assume its *vev*, *i.e.* $s(0) \neq 1$, *cf.* Eq. (5). This changes the kinematical quantities in Eq. (A.3) of the regular solution to

$$f_i^{(0)}(r) = J_\alpha(qr) \qquad \text{and} \qquad g_i^{(0)}(r) = \zeta\, J_\beta(qr)\,, \tag{A.25}$$

where

$$q^2 = \epsilon^2 - m^2 s^2(0) \qquad \text{and} \qquad \zeta^2 = \frac{\epsilon - m s(0)}{\epsilon + m s(0)}\,. \tag{A.26}$$

Working out the Wronskian yields the following correction for the logarithmic Jost function and its Born series [32],

$$\begin{aligned}
\nu_F(t) &\equiv \widetilde{\nu}_F(t) + 2\,\ln\left(\frac{\tau - im}{\tau - ims(0)}\right) & \nu_G(t) &\equiv \widetilde{\nu}_G(t) + 2\,\ln\left(\frac{\tau + im}{\tau + ims(0)}\right) \\
\nu_F^{(1)}(t) &\equiv \widetilde{\nu}_F^{(1)}(t) + 2\,\frac{1 - s(0)}{1 + i\,\tau/m} & \nu_G^{(1)}(t) &\equiv \widetilde{\nu}_G^{(1)}(t) + 2\,\frac{1 - s(0)}{1 - i\,\tau/m} \\
\nu_F^{(2)}(t) &\equiv \widetilde{\nu}_F^{(2)}(t) + \left(\frac{1 - s(0)}{1 + i\,\tau/m}\right)^2 & \nu_G^{(2)}(t) &\equiv \widetilde{\nu}_G^{(2)}(t) + \left(\frac{1 - s(0)}{1 - i\,\tau/m}\right)^2\,,
\end{aligned} \tag{A.27}$$

where $\tau = \sqrt{t^2 - m^2}$ and the factor two arises because there are four channels: $\ln\zeta^4 = 2\ln\zeta^2$.

With these modifications we find that $\nu_F(t)$ and $\nu_G(t)$ are indeed real and identical. This is also true at any order in the Born series. The pseudo-scalar profile component does not contribute to the correction because $p(0) = 0$.

Appendix B. Feynman diagrams

The Feynman diagrams are generated by the expansion of the fermion determinant

$$\begin{aligned}\mathcal{A} \equiv -T L_z \mathcal{E}_F &= (-i)\, N_c\, \ln\det\,(-\partial\!\!\!/ - m - V) \\ &= (-i)\, N_c\, \ln\det\,(\partial\!\!\!/ - m) + i N_c \sum_{n=1}^{\infty} \frac{1}{n} \mathrm{Tr}\left[\left(i\partial\!\!\!/ - m\right)^{-1} V\right]^n \equiv \sum_{n=0}^{\infty} \mathcal{A}_n\,,\end{aligned} \tag{B.1}$$

where $V = \beta H_{\rm int}$ is the interaction potential from Eq. (13). The first-order ($n = 1$) diagram is *local* and can be eliminated completely by a counterterm of the form

$$\mathcal{L}_{CT} = c_3 \left[\mathrm{tr}(\Phi^\dagger \Phi) - 2v^2\right]$$

which contains $s(r) - 1$, $[s(r) - 1]^2$ and $p^2(r)$ terms. The linear term eliminates the tadpole and keeps the Higgs *vev* at its classical value. The quadratic terms serve to renormalize $\mathcal{A}_2$, together with the quadratic part of the second counterterm

$$\mathcal{L}_{CT} = c_4 \left[\mathrm{tr}(\Phi^\dagger \Phi) - 2v^2\right]^2. \tag{B.2}$$

This counterterm also contains pieces cubic and quartic in the profiles. They renormalize the third- and fourth-order diagram below. Choosing the no-tadpole scheme for $\mathcal{A}_1$ and $\overline{MS}$ for $\mathcal{A}_2$ yields

$$\begin{aligned}\mathcal{E}^{(2)}_{\rm FD}\Big|_{\overline{MS}} &\equiv \frac{-1}{T L_z}\left[\mathcal{A}_1 + \mathcal{A}_2\right] \\ &= -N_c \int_0^\infty \frac{dk\, k}{4\pi}\, I_1(k/m) \left(4m^2 \widetilde{\alpha}_H(k)^2 + k^2\left[\widetilde{\alpha}_H(k)^2 + \widetilde{\alpha}_P(k)^2\right]\right)\end{aligned} \tag{B.3}$$

with the explicit parameter integral

$$I_1(t) \equiv \int_0^1 dx\, \ln\left[1 + x(1-x)\, t^2\right] = \frac{2}{t}\sqrt{4 + t^2}\,\mathrm{arcsinh}(t/2) - 2 \tag{B.4}$$

and the Fourier–Bessel transform of the background potential

$$\widetilde{\alpha}_H(k) = m \int_0^\infty dr\, r\, J_0(kr)\left[s(r) - 1\right] \tag{B.5}$$

$$\widetilde{\alpha}_P(k) = m \int_0^\infty dr\, r\, J_1(kr)\, p(r)\,. \tag{B.6}$$

The contribution quadratic in $\widetilde{\alpha}_P(k)$ starts with a prefactor k^2, *i.e.* the pseudo-scalar excitations remain massless.

The third- and fourth-order diagrams are more complicated. Fortunately, within the fake boson method, *cf.* the following appendix, we only need to identify their (logarithmic) divergences

$$\left[\mathcal{A}_3+\mathcal{A}_4\right]=i\,\pi\,c_F\,TL_z\,\mu^{4-D}\int\frac{d^Dk}{(2\pi)^D}\,(k^2-m^2+i0)^{-2}+\ldots\,, \tag{B.7}$$

where D is the number of spacetime dimensions in dimensional regularization and the ellipsis indicates finite pieces. Since the only counterterm for these diagrams is Eq. (B.2) and the coefficient c_4 has already been determined by the second-order diagram above, we can predict c_F directly if we assume that the theory is renormalizable. Alternatively, we can compute c_F from the divergence of the third- and fourth-order diagram, which yields the same expression

$$c_F=4m^4N_c\int_0^\infty dr\,r\left[\,(s(r)-1)^2+p^2(r)\right]\left[(s(r)-1)^2+p^2(r)+4s(r)-4\right] \tag{B.8}$$

where the prefactor four results from the Dirac trace.

Appendix C. Fake boson subtraction

The second-order Feynman diagram of a scalar boson scattering off a radially symmetric background potential $V_B(r)$ is logarithmically divergent. By proper rescaling it replaces the third- and fourth-order fermion diagrams and Born subtractions. To be specific, we choose a one-parameter profile

$$V_B(r)\equiv m^2\frac{r}{w_B}\exp\left(-2\frac{r}{w_B}\right), \tag{C.1}$$

where w_B is an arbitrary width which should not play a role in the final result. The logarithmic divergence of the second-order contribution to the effective action

$$\begin{aligned}\mathcal{A}_2^{(\infty)}&=i\,\pi\,c_B\,TL\mu^{4-D}\int\frac{d^Dq}{(2\pi)^D}\,(q^2-m^2+i0)^{-2}\\ c_B&\equiv-\frac{1}{2}\int_0^\infty dr\,r\,V_B(r)^2=-\frac{3m^4\,w_B^2}{256}\,,\end{aligned} \tag{C.2}$$

where μ is an arbitrary renormalization scale introduced by dimensional regularization to D spacetime dimensions. This should be compared to the corresponding expression Eq. (B.7) from the third- and fourth-order fermion diagrams. Employing the $\overline{MS}$ scheme, the renormalized energy per unit length is

$$\mathcal{E}_B^{(2)}\Big|_{\overline{MS}}=+\frac{1}{32\pi}\int_0^\infty dq\,q\,I_1(q)\,\overline{V}_B(q)^2, \tag{C.3}$$

where I_1 is given in Eq. (B.4) and $q\equiv k/m$ is dimensionless. The Fourier transform of the background is also dimensionless

$$\overline{V}_B(q)\equiv\int_0^\infty dr\,r\,V_B(r)\,J_0(qmr)=(\widehat{w}_B)^2\frac{8-(\widehat{w}_Bq)^2}{\left[4+(\widehat{w}_Bq)^2\right]^{\frac{5}{2}}}\,, \tag{C.4}$$

where $\widehat{w}_B\equiv mw_B$ is the fake boson profile width measured in inverse units of the fermion mass m.

The second-order Born approximation, $\overline{v}_\ell^{(2)}(k)$, to the logarithm of the Jost function for a scalar boson scattering off the background V_B can be computed by standard techniques, *cf.* Ref. [41]. After analytic continuation to the imaginary axis it gives rise to the function

$$u_B^{(2)}(t) \equiv \sum_{\ell=0}^{\infty} [2 - \delta_{\ell 0}]\, \overline{v}_\ell^{(2)}(it)\,, \tag{C.5}$$

which enters Eq. (22) and produces a finite spectral integral in Eq. (21). Numerically we have verified invariance of the vacuum polarization energy, Eq. (26) with respect to the artificial width parameter w_B.

Appendix D. On-shell renormalization scheme

All finite counterterm contributions contain pieces from the classical Lagrangian with finite coefficients,

$$\Delta\mathcal{E}_{\rm ren} = N_c \int_0^\infty dr\, r \left\{ \overline{c}_2 \left[s'(r)^2 + p'(r)^2 + \frac{p(r)^2}{r^2} \right] + \overline{c}_4 \left[1 - s(r)^2 - p(r)^2 \right]^2 \right\}, \tag{D.1}$$

where the prime denotes the derivative with respect to the radial coordinate r. When passing from the $\overline{MS}$ to the physical *on-shell* scheme, the finite coefficients $\overline{c}_2$ and $\overline{c}_4$ are determined such that the renormalized Higgs propagator has a pole at $4\lambda v^2$ with unit residue. The general expressions are readily taken from Ref. [32]. Fortunately they simplify considerably for the case of the hedgehog string,

$$\overline{c}_2 = \frac{1}{\pi}\left[\frac{1}{3} + 3\, I_2(i\mu_H)\right] \qquad \text{and} \qquad \overline{c}_4 = \frac{1}{4\pi}\left[\mu_H^2 + 6\, I_1(i\mu_H)\right] \tag{D.2}$$

where $I_1(i\mu_H)$ is given in Eq. (B.4), $\mu_H = m_H/m = 2\sqrt{\lambda}/f$, and

$$\begin{aligned} I_2(i\mu) &= \int_0^1 dx\, x(1-x) \ln\left[1 - x(1-x)\,\mu^2\right] \\ &= -\frac{\mu(12+5\mu^2)\sqrt{4-\mu^2} + 6(\mu^4 - 2\mu^2 - 8)\,\arcsin(\mu/2)}{18\mu^3\sqrt{4-\mu^2}}\,. \end{aligned} \tag{D.3}$$

Appendix E. Bound states

In this appendix we describe the computation of the single particle bound state energies, $\epsilon_{i,\ell}$. We follow Ref. [32] and diagonalize the interaction Hamiltonian, Eq. (11) in the free grand spin basis used in Appendix A, *cf.* Eqs. (A.2) and (A.3). The discretized momenta $k_n^{(\ell)}$ in the angular momentum channel ℓ are determined such that no flux emerges from the string core through a large circle of radius R around the core. The flux combines upper and lower components of the spinor in Eq. (A.2) and vanishes when any of them is zero. From Eq. (A.3) it is obvious that the most compact condition is

$$J_{\ell+1}(k_n^{(\ell)} R) = 0\,, \qquad n = 1, 2, \ldots\,.$$

Since for any given ℓ there is only one set of discretized momenta, we will omit that label for simplicity.

We impose a numerical cutoff Λ such that only the $k_n < \Lambda$ are included in the basis. The total number N of such momenta k_n depends on both the angular momentum channel ℓ and the size of the radius R. For each momentum k_n there are two, which we sort in ascending order:

$$\epsilon_n^{(0)} = \begin{cases} -\sqrt{k_{N+1-n}^2 - m^2} & : \quad n = 1, \ldots, N \\ +\sqrt{k_{n-N}^2 - m^2} & : \quad n = N+1, \ldots, 2N\,. \end{cases} \tag{E.1}$$

The free Hamiltonian, Eq. (12), exhibits a four-fold degeneracy from spin and isospin invariance, which we assemble into a single super-index that has two entries $\alpha = (n, i)$ with $i = 1, 2, 3, 4$, according to Eq. (A.2). The interaction matrix elements are worked out explicitly using the super-indices $\alpha = (n, i)$ and $\beta = (m, j)$

$$\begin{aligned} \hat{V}_{(n,i)(m,j)} &= \langle ni \,|\, H_{\text{int}} \,|\, mj \rangle \\ &= \delta_{ij} \int_0^R dr\, r \left[f_i^{(0)}(k_n r)\, f_j^{(0)}(k_m r) - g_i^{(0)}(k_n r)\, g_j^{(0)}(k_m r) \right] \\ &\quad + \sigma_{ij} \int_0^R dr\, r \left[f_i^{(0)}(k_n r)\, g_j^{(0)}(k_m r) - g_i^{(0)}(k_n r)\, f_j^{(0)}(k_m r) \right], \end{aligned} \tag{E.2}$$

where $f_i^{(0)}$ and $g_i^{(0)}$ are the radial functions from Eq. (A.3) with momenta k_n and

$$\sigma_{ij} = \begin{pmatrix} 0 & 0 & 0 & +1 \\ 0 & 0 & -1 & 0 \\ 0 & +1 & 0 & 0 \\ -1 & 0 & 0 & 0 \end{pmatrix}.$$

Numerical diagonalization of the symmetric $8N \times 8N$ matrix $\hat{H} = \hat{H}_0 + \hat{V}$ ($\hat{H}_0$ is a diagonal matrix that contains four copies of $\epsilon_n^{(0)}$) yields $8N$ eigenvalues $\epsilon_{(n,i)}$. Those with $|\epsilon_{(n,i)}| < m$ are stable against changes of sufficiently large Λ or R and are identified as the true bound state energies. The numerical tests in section 4 indicate that $\Lambda \approx 10m$ and $R \approx 80/m$, which corresponds to $N \approx 250$, can be considered sufficiently large for all contributing angular momentum channels ℓ. In that case we have to diagonalize a 2000×2000 matrix in every angular momentum channel.

References

[1] T. Vachaspati, Phys. Rev. Lett. 68 (1992) 1977;
T. Vachaspati, Phys. Rev. Lett. 69 (1992) 216 (Erratum).
[2] A. Achucarro, T. Vachaspati, Phys. Rep. 327 (2000) 347.
[3] Y. Nambu, Nucl. Phys. B 130 (1977) 505.
[4] M.B. Hindmarsh, T.W.B. Kibble, Rep. Prog. Phys. 58 (1994) 477.
[5] T.W.B. Kibble, J. Phys. A 9 (1976) 1387.
[6] E.P.S. Shellard, A. Vilenkin, Cosmic Strings and Other Topological Defects, Cambridge University Press, Cambridge, UK, 1994.
[7] E.J. Copeland, T.W.B. Kibble, Proc. R. Soc. Lond. A 466 (2010) 623.
[8] A. Achucarro, C.J.A. Martins, arXiv:0811.1277 [astro-ph].
[9] R.H. Brandenberger, A. Davis, Phys. Lett. B 308 (1993) 79;
R.H. Brandenberger, A. Davis, M. Trodden, Phys. Lett. B 335 (1994) 123.

[10] K. Kajantie, M. Laine, K. Rummukainen, M.E. Shaposhnikov, Phys. Rev. Lett. 77 (1996) 2887;
K. Rummukainen, M. Tsypin, K. Kajantie, M. Laine, M.E. Shaposhnikov, Nucl. Phys. B 532 (1998) 283;
F. Csikor, Z. Fodor, J. Heitger, Phys. Rev. Lett. 82 (1999) 21.
[11] C. Grojean, G. Servant, J.D. Wells, Phys. Rev. D 71 (2005) 036001;
A. Menon, D.E. Morrissey, C.E.M. Wagner, Phys. Rev. D 70 (2004) 035005.
[12] M. Sato, Phys. Lett. B 376 (1996) 41.
[13] J. Dziarmaga, Phys. Rev. D 52 (1995) 569.
[14] J.M. Cline, J.R. Espinosa, G.D. Moore, A. Riotto, Phys. Rev. D 59 (1999) 065014.
[15] E. D'Hoker, E. Farhi, Nucl. Phys. B 248 (1984) 59;
E. D'Hoker, E. Farhi, Nucl. Phys. B 248 (1984) 77.
[16] E. Witten, Nucl. Phys. B 249 (1985) 557.
[17] S.G. Naculich, Phys. Rev. Lett. 75 (1995) 998.
[18] F.R. Klinkhamer, C. Rupp, J. Math. Phys. 44 (2003) 3619.
[19] G. Starkman, D. Stojkovic, T. Vachaspati, Phys. Rev. D 65 (2002) 065003;
G. Starkman, D. Stojkovic, T. Vachaspati, Phys. Rev. D 63 (2001) 085011;
D. Stojkovic, Int. J. Mod. Phys. A 16S1C (2001) 1034.
[20] M. Groves, W.B. Perkins, Nucl. Phys. B 573 (2000) 449.
[21] H. Weigel, M. Quandt, Phys. Lett. B 690 (2010) 514.
[22] H. Weigel, M. Quandt, N. Graham, Phys. Rev. D 94 (2016) 045015.
[23] H.B. Nielsen, P. Olesen, Nucl. Phys. B 61 (1973) 45.
[24] M. Bordag, I. Drozdov, Phys. Rev. D 68 (2003) 065026.
[25] J. Baacke, N. Kevlishvili, Phys. Rev. D 78 (2008) 085008.
[26] M. Lilley, F. Di Marco, J. Martin, P. Peter, Phys. Rev. D 82 (2010) 023510.
[27] R.L. Davis, E.P.S. Shellard, Phys. Lett. B 209 (1988) 485;
Y. Lemperiere, E.P.S. Shellard, Phys. Rev. Lett. 91 (2003) 141601.
[28] M. Quandt, N. Graham, H. Weigel, Phys. Rev. D 87 (2013) 085013.
[29] M. Nagasawa, R.H. Brandenberger, Phys. Lett. B 467 (1999) 205;
M. Nagasawa, R. Brandenberger, Phys. Rev. D 67 (2003) 043504;
J. Karouby, R. Brandenberger, Phys. Rev. D 85 (2012) 107702.
[30] P. Forgács, Á. Lukács, Phys. Rev. D 95 (2017) 035003.
[31] H. Weigel, M. Quandt, N. Graham, Phys. Rev. Lett. 106 (2011) 101601.
[32] N. Graham, M. Quandt, H. Weigel, Phys. Rev. D 84 (2011) 025017.
[33] T.H.R. Skyrme, Proc. R. Soc. Lond. A 260 (1961) 127;
T.H.R. Skyrme, Int. J. Mod. Phys. A 3 (1988) 2745, article reconstructed by I. Aitchison.
[34] R. Alkofer, H. Reinhardt, H. Weigel, Phys. Rep. 265 (1996) 139.
[35] N. Graham, M. Quandt, H. Weigel, Lect. Notes Phys. 777 (2009) 1.
[36] J.S. Faulkner, J. Phys. C 10 (1977) 4661.
[37] R.D. Puff, Phys. Rev. A 11 (1975) 154.
[38] N. Graham, R.L. Jaffe, M. Quandt, H. Weigel, Ann. Phys. 293 (2001) 240.
[39] N. Graham, R.L. Jaffe, M. Quandt, H. Weigel, Phys. Rev. Lett. 87 (2001) 131601.
[40] R.G. Newton, Scattering Theory of Waves and Particles, Springer, New York, 1982;
K. Chadan, P.C. Sabatier, Inverse Problems in Quantum Scattering Theory, Springer, New York, 1989.
[41] N. Graham, R.L. Jaffe, V. Khemani, M. Quandt, M. Scandurra, H. Weigel, Nucl. Phys. B 645 (2002) 49.
[42] H. Weigel, M. Quandt, N. Graham, O. Schröder, Nucl. Phys. B 831 (2010) 306.
[43] G. Ripka, S. Kahana, Phys. Rev. D 36 (1987) 1233.